

AD-A122 540

ACOUSTIC NDE OF MULTILAYERED COMPOSITES PHASE I
ACOUSTIC MODEL DEVELOPMENT..(U) TETRA TECH INC ARLINGTON
VA R SHANKAR ET AL. 22 JUL 82 TETRAT-A-6139

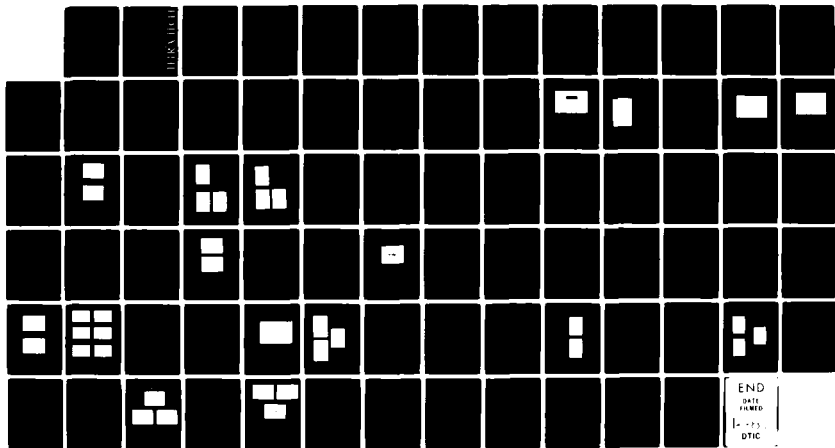
1/

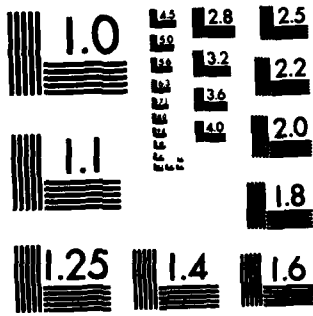
UNCLASSIFIED

N60921-81-C-0300

F/G 14/2

NL





MICROCOPY RESOLUTION TEST CHART
NATIONAL BUREAU OF STANDARDS-1963-A

AD A 122540

12

ACOUSTIC NDE OF MULTILAYERED COMPOSITES

PHASE I: ACOUSTIC MODEL DEVELOPMENT AND INSPECTION OF BRONZE-RUBBER STRUCTURES

22 JULY 1982

SDIC
ELECTE
DEC 17 1982
A

DTIC FILE COPY

This document has been approved for public release and sale; its distribution is unlimited.

82 12 17 023

TETRA TECH

TC-6139

ACOUSTIC NDE OF MULTILAYERED COMPOSITES

PHASE I: ACOUSTIC MODEL DEVELOPMENT AND
INSPECTION OF BRONZE-RUBBER STRUCTURES

FINAL TECHNICAL REPORT

Prepared Under Contract N-60921-81-C-0300

Period Covered: September 1981 - June 1982

Prepared by:

Ramesh Shankar, Ph.D.
Stephen S. Lane, Ph.D.
Thomas J. Paradiso

Tetra Tech, Inc.
1911 N. Ft. Myer Drive
Arlington, Virginia 22209

This document has been approved
for public release and sale, in
whole or in part, by the
National Technical Information Administration

REPORT DOCUMENTATION PAGE		READ INSTRUCTIONS BEFORE COMPLETING FORM
1. REPORT NUMBER	2. GOVT ACCESSION NO. AD-A122540	3. RECIPIENT'S CATALOG NUMBER
4. TITLE (and Subtitle) Acoustic NDE of Multilayered Composites Phase I: Acoustic Model Development and Inspection of Bronze-Rubber Structures		5. TYPE OF REPORT & PERIOD COVERED Final Report for Period 9/25/81-3/25/82
		6. PERFORMING ORG. REPORT NUMBER PC-6139
7. AUTHOR(s) Ramesh Shankar Stephen S. Lane Thomas J. Paradiso		8. CONTRACT OR GRANT NUMBER(s) N-60921-81-C-0300
9. PERFORMING ORGANIZATION NAME AND ADDRESS Tetra Tech, Inc. 1911 N. Ft. Myer Drive, Suite 601 Arlington, VA 22209		10. PROGRAM ELEMENT, PROJECT, TASK AREA & WORK UNIT NUMBERS
11. CONTROLLING OFFICE NAME AND ADDRESS Naval Surface Weapons Center White Oak, MD 20910 Code: R34, Materials Evaluation		12. REPORT DATE July 1982
		13. NUMBER OF PAGES 71
14. MONITORING AGENCY NAME & ADDRESS (if different from Controlling Office)		15. SECURITY CLASS. (of this report) UNCLASSIFIED
		15a. DECLASSIFICATION/DOWNGRADING SCHEDULE
16. DISTRIBUTION STATEMENT (of this Report) Approved for Public Release; Distribution Unlimited.		
17. DISTRIBUTION STATEMENT (of the abstract entered in Block 20, if different from Report)		
18. SUPPLEMENTARY NOTES		
19. KEY WORDS (Continue on reverse side if necessary and identify by block number) Nondestructive Evaluation, Multilayered Structures, Acoustic Modeling, Lattice Filter, Angled Beam Inspection, Attenuation, Mode Conversion, Digital Data Acquisition, Signal Processing, Filtering, Deconvolution, Cepstral Filtering		
20. ABSTRACT (Continue on reverse side if necessary and identify by block number) Development of a consistent and methodological approach to the nondestructive evaluation (NDE) of multilayered structures is of primary importance to the U.S. Navy to improve fleet reliability. Consequently, a project was initiated with Tetra Tech to develop a generic, computer-based acoustic model, and to validate model on bronze-rubber specimen structures by collecting and processing ultrasonic digital data. The report details work performed on the project. <p style="text-align: right;">(continued on reverse)</p>		

UNCLASSIFIED

SECURITY CLASSIFICATION OF THIS PAGE (When Data Entered)

The computer based model, written in FORTRAN IV for a general purpose computer, is applicable for normal or off-normal incident excitation, with receiver in pulse-echo, pitch-catch or in array mode. The model can simulate the observed signal for arbitrary frequency response of the transmitting and receiving transducer. In addition the model considers attenuative and mode conversion effects in each layer in predicting the ultrasonic response.

Ultrasonic digital data were processed from a bronze-epoxy-rubber multilayered structure to validate model and to determine suitable digital signal processing methods. These methods included: compensating filters which were frequency dependent to offset attenuation in the media; deconvolution for bandwidth enhancement and to improve resolution, and the cepstrum -- a relatively new method -- to separate the overlapped response from different interfaces.

Computer model simulation was used successfully to predict the response from this structure. In particular, the model output dictated the inspection configuration and signal processing methods to be used on the data.

Accession For
INDEXED
FILED
SEARCHED
SERIALIZED

A

DTIC
COPY
RESPECTED

UNCLASSIFIED

SECURITY CLASSIFICATION OF THIS PAGE (When Data Entered)

FOREWORD

This final report covers work performed during the period September 25, 1981 through May 25, 1982 under Contract N-60921-C-0300, "Acoustic NDE of Multilayered Composites."

Mr. Cliff Anderson, R34, was the program monitor. The authors thank Mr. Anderson for his guidance. The contributions of Mr. Jeffrey M. Warren and Dr. Palmer L. Edwards, R34, in collecting and digitizing data and providing information on the multilayered samples are gratefully acknowledged.

Dr. Ramesh Shankar, Tetra Tech, was the program manager and principal investigator.

ABSTRACT

Development of a consistent and methodological approach to the nondestructive evaluation (NDE) of multilayered structures is of primary importance to the U.S. Navy to improve fleet reliability. Consequently, a project was initiated with Tetra Tech to develop a generic, computer-based acoustic model, and to validate model on bronze-rubber specimen structures by collecting and processing ultrasonic digital data. The report details work performed on the project.

The computer based model, written in FORTRAN IV for a general purpose computer, is applicable for normal or off-normal incident excitation, with receiver in pulse-echo, pitch-catch or in array mode. The model can simulate the observed signal for arbitrary frequency response of the transmitting and receiving transducer. In addition the model considers attenuative and mode conversion effects in each layer in predicting the ultrasonic response.

Ultrasonic digital data were processed from a bronze-epoxy-rubber multilayered structure to validate model and to determine suitable digital signal processing methods. These methods included: compensating filters which were frequency dependent to offset attenuation in the media; deconvolution for bandwidth enhancement and to improve resolution, and the cepstrum -- a relatively new method -- to separate the overlapped response from different interfaces.

Computer model simulation was used successfully to predict the response from this structure. In particular, the model output dictated the inspection configuration and signal processing methods to be used on the data.

TABLE OF CONTENTS

	Page
SUMMARY OF RESULTS AND RECOMMENDATIONS.....	v
INTRODUCTION AND OBJECTIVES.....	1
Objectives.....	3
Report Organization.....	3
MULTILAYER MODEL DEVELOPMENT.....	4
Introduction.....	4
Wave Equations at an Interface.....	4
Lattice Filter Representation.....	5
Simulation for Bronze-Rubber Structure.....	12
Incorporation of a Flaw in Model.....	15
Effects of Attenuation.....	18
Propagation at Off-Normal Incidence.....	26
ULTRASONIC DATA COLLECTION.....	37
Introduction.....	37
Bronze-Rubber Specimens.....	37
Apparatus and Ultrasonic Data Collection.....	40
ULTRASONIC SIGNAL PROCESSING.....	44
Introduction.....	44
Filtering.....	44
Deconvolution.....	48
Cepstral Processing.....	57
Conclusions.....	63
SUMMARY OF RESULTS AND RECOMMENDATIONS.....	65
REFERENCES.....	66
APPENDIX: FLOW CHART OF ACOUSTIC NDE COMPUTER MODEL	67

LIST OF FIGURES

	Page
Figure 3.1 Reflection and Transmission Across a Boundary.....	6
Figure 3.2 Ray Tracing for a Two Layered Structure	7
Figure 3.3 Wave Equation at Interface	9
Figure 3.4 Lattice Representation of Wave at Interface ..	11
Figure 3.5 Bronze-Rubber Multilayer Structure	13
Figure 3.6 Reflection Series from Good Specimen	14
Figure 3.7 Transducer Impulse Response	16
Figure 3.8 Simulated Response with 5.0 MHZ Transducer and SNR=40dB	17
Figure 3.9 Top of Rubber Layer	19
Figure 3.10 Bottom of Rubber Layer	19
Figure 3.11 Attenuation in Bronze	21
Figure 3.12 Attenuation in Rubber	22
Figure 3.13 Angle Beam Inspection	27
Figure 3.14 Reflection Coefficients Bronze Rubber Interface	32
Figure 3.15 Effect of Phase Shift on Waveform	34
Figure 3.16 Effect of Phase Shift in Angled Beam Impulse Response	35
Figure 4.1 Bronze Rubber Multilayered Specimen	38
Figure 4.2 Positions where Ultrasonic Data were Recorded.	39
Figure 4.3 Ultrasonic Digital Data Processing Configuration	41
Figure 4.4 Header Sheet	42
Figure 5.1 FIR Bandpass Filter	46
Figure 5.2 Original Trace	47
Figure 5.3 FIR Filtered	47
Figure 5.4 Conventional Filtering	47
Figure 5.5 Frequency Compensating Filter	49
Figure 5.6 Front and Back Surface Response	50
Figure 5.7 Frequency-Compensating Filtering	51
Figure 5.8 Steps in Deconvolution	53
Figure 5.9 Deconvolution for Increased Resolution	54
Figure 5.10 Increased Resolution in Bronze-Rubber Inspection by Deconvolution	55
Figure 5.11 Deconvolution of Bronze Reverberations	56
Figure 5.12 Minimization of Bronze Reverberations	58
Figure 5.13 Steps in Complex Cepstrum Computation	60
Figure 5.14 Complex Cepstrum Filtering	61
Figure 5.15 Cepstrum Processing	62
Figure 5.16 Correlation of Recovered Signal and Echo	64

SUMMARY OF RESULTS AND RECOMMENDATIONS

A computer based acoustic model has been developed for the NDE of multilayered structures. The model is applicable for normal or off-normal incident excitation, with receiver in pulse-echo, pitch-catch or in array mode. The model can simulate the observed signal for arbitrary frequency response of the transmitting and receiving transducer. In addition the model considers attenuative and mode conversion effects in each layer in predicting the ultrasonic response.

Ultrasonic digital data were processed from a bronze-epoxy-rubber multilayered structure to validate model and to determine suitable digital signal processing methods. These methods included: compensating filters which were frequency dependent to offset attenuation in the media; deconvolution for bandwidth enhancement and to improve resolution, and the cepstrum -- a relatively new method -- to separate the overlapped response from different interfaces.

Computer model simulation was used successfully to predict the response from this structure. In particular, the model output dictated the inspection configuration and signal processing methods to be used on the data.

Based on these results, it is recommended that angled beams be used to inspect the structures instead of the traditional normal incidence, pulse-echo methods used. It is further recommended that validation of the angled beam model be carried out by analyzing and processing digital data from these structures.

INTRODUCTION AND OBJECTIVES

BACKGROUND AND OVERVIEW

The US Navy has embarked on a comprehensive program to evaluate by nondestructive methods the integrity of multilayered structures. These structures include use of conventional materials--such as those in metal-to-metal lap joints, pavements, and ship bulkheads--as well as advanced materials such as carbon-carbon composites and rubber-bronze composites. The physical dimensions of these structures vary from several feet (pavements) to few thousandths of an inch (carbon-carbon composites). Subsurface flaws within these structures, especially at their interfaces, compromise safe operation of these structures. Underground voids in pavements, and contaminants, voids, inclusions, and delaminations of composite materials are a few examples of the expected types of flaws [1].

A variety of NDE methods are currently employed. These range from the use of resistivity and seismic surveying method for pavement inspection [2] to ultrasonic and eddy current methods for composite materials [1]. Acoustic methods are the most popular due to their easy deployment, low power requirements and general repeatability.

In order to develop a consistent and methodological approach to acoustic NDE of multilayered structures, the US Navy initiated the first phase of a project with Tetra Tech to develop and validate a generic computer-based model, with validation to be performed on a specific bronze-rubber multilayered structure. The primary aim of the modeling effort was to derive the response at any intermediate layer for an arbitrary acoustic source with the beam incident at an arbitrary angle to the surface. By incorporating a flaw into the model (such as a delamination) its effects on the total response could be determined.

The basis for the model was established by Robinson and Treitel [3] and Ewing, Jardetsky, and Press [4] for geophysical prospecting and by Scott [5] for acoustic inspection of multilayered structures. While the earlier efforts considered normal incidence and non attenuative media, work under this project expanded its capabilities to include off-normal incident angles and the attendant mode conversions created with this inspection configuration. For the latter case, the reflection and transmission coefficients at each interface are in general complex quantities, obtained by

solving a matrix equation. An additional model feature is provision for including the effects of attenuation within each layer. It can be modeled as a constant over all frequencies or as a frequency-dependent quantity, such as a constant "Q" model. Common materials such as aluminum, stainless steel, rubber and biological tissues exhibit this property.

While modeling the acoustical behavior of multilayered structures is important in understanding the physics, an additional, complementary problem in acoustic NDE is signal interpretation. The signals observed at the surface will consist of a confusing series of reflections from different layers as well as reverberations within a layer. These signals have finite resolution due to finite transducer bandwidth, further confusing the arrival times because of signal overlap. Specialized signal processing methods are required to correctly identify the signal response at a particular layer. The model allows the user to examine separately the effects due to the layered structure and that due to the flaw itself. Appropriate signal processing methods can then be utilized for the theoretical waveform which maximize the flaw response and minimize the reverberation effects due to the multiple layers. Predictive deconvolution [4], and cepstral methods [5] are techniques that have found use in several, similar applications.

The full benefit of modeling can be realized then by first evaluating these signal processing methods on simulated data, analyzing their performance, and then applying them to actual inspection data. Knowledge gained from the simulation would include proper choice of frequency, appropriate instrumentation, experimental design, and post signal processing methods for use on the multilayered structure of interest.

Model validation was performed on alternating layers of bronze and rubber structures whose dimensions were such as to cause approximately equal acoustic transit times within each. An additional problem was that rubber, being fairly attenuative, prevented sufficient energy from penetrating into the deeper layers for inspecting delaminations. This was especially acute for the higher frequencies which would have provided the necessary resolution for inspection. The problem of overlapping returns from successive bronze and rubber layers can be overcome by inspecting with angled beams. However, angulating the beam would create different modes of wave propagations within each layer; each mode will be reflected or transmitted at an interface. Sorting these different modes in a methodical manner is one of the benefits of such a model. This formed the basis for recommending future efforts in developing and validating the model for angled beam inspection.

OBJECTIVES

The objectives of the project as described in the work statement were to:

- o develop an acoustic model for multilayered structures
- o design experiments for ultrasonic data collection from rubber-bronze specimens.

The model has been simulated on an in-house minicomputer and requires as inputs basic acoustic parameters related to the multilayered structure. The acoustic response can be simulated for a variety of inspection conditions (pulse-echo, pitch-catch, through-transmission, or synthetic array), transducer driver functions (pulsed, pseudo-random or CW), and signal-to-noise ratios.

REPORT ORGANIZATION

The next section contains description of the multilayered model development starting from normal incidence, plane wave propagation in non-attenuative media to off-normal beam incidence in attenuative media. It is shown that a cascaded, lattice filter representation [3] can be used to model the layered response. The elements of the lattice filter are scalar quantities for normal incidence waves in non-attenuative media and a vector for attenuative media and/or off-normal incident waves. The response under these different conditions are fully developed for a multilayered bronze-rubber structure with and without epoxy (i.e. flaw) in intermediate layers.

Section 4 contains description of the ultrasonic data collection apparatus and procedures used on bronze-rubber composite specimens. The procedures were based partly on theoretical findings documented in the previous section.

A narration can be found in Section 5 of signal processing procedures used on both theoretical and actual data to enhance the response from different layers. In particular, it is shown how frequency-dependent compensating filters and deconvolution methods can be used to increase resolution and separate overlapped signals from intermediate layers.

A flow chart and description of the computer program which generates the reflection series can be found in the Appendix.

MULTILAYER MODEL DEVELOPMENT

INTRODUCTION

The basic problem to be solved by the multilayered model is the prediction of the response from an arbitrary layered structure when interrogated by an ultrasonic pulse. The model output must be a time domain waveform, corresponding to the measured waveform at the terminals of a real transducer, in response to a specified pulse of ultrasonic energy incident on the layered structure. All relevant effects, such as reflection, refraction, mode conversion and attenuation, must be included.

WAVE EQUATIONS AT AN INTERFACE

To solve this problem, the effect of an ultrasonic wave when it impinges on a boundary must be known. Calculation of these effects has been presented in a number of texts; i.e., Ewing, Jardetzky and Press [4]. The results will be summarized here. First, normal incidence wave is considered. The case where the angle between the direction of propagation and the layer is arbitrary will be taken up in a later section.

In general, waves of any sort are partly reflected and partly transmitted at a boundary. In the ultrasonic case in solids two wave types are possible, but for normal incidence there is no conversion from one type to the other, hence this can be treated independently. If the amplitude of the incident wave is taken to be unity, then the amplitude of the reflected wave will less than/or equal to unity, and may be reversed in sign from that of the incident wave. The amplitude of the transmitted wave may be greater or less than unity, but its sign will always be that of the incident wave. The reflection coefficient is defined as the ratio of the amplitude of the reflected wave to that of the incident wave. Its absolute value is one or less. Similarly, the transmission coefficient is defined to be the ratio of the transmitted to incident amplitudes.

If the velocity of the phase in question is V and the density of the material through which it propagates is ρ , then the acoustic impedance is defined to be $Z=V\rho$. Z depends on the medium, so it will be given a subscript to indicate the layer to which it applies. It depends on the wave type through the velocity V .

Figure 3.1 shows an interface between medium 1 above, with acoustic impedance Z_1 , and medium 2 below, with acoustic impedance Z_2 . A wave is incident on the interface from medium 1. In [4] it is shown that the reflection coefficient R_{12} is equal to

$$R_{12} = \frac{Z_2 - Z_1}{Z_1 + Z_2} \quad 3.1$$

and that the transmission coefficient T_{12} is equal to

$$T_{12} = \frac{2 Z_1}{Z_1 + Z_2} \quad 3.2$$

If Z_2 is greater than Z_1 , then R is negative, corresponding to reflection with a change in sign. T is less than one in this case. However, if Z_2 is less than Z_1 , T is greater than one. The amplitude of the transmitted wave is thus greater than that of the incident wave. Consideration of the energy in each wave shows that conservation of energy is not violated, however.

For waves incident on the boundary from medium 2, the role of Z_1 and Z_2 in equations 3.1 and 3.2 are interchanged.

For any boundary, we have the following:

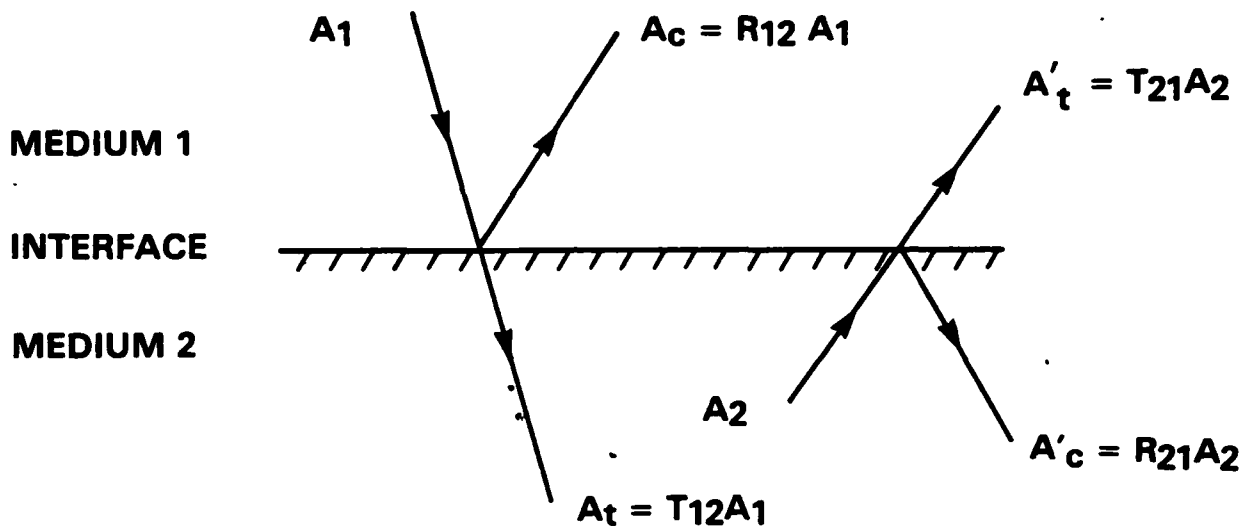
$$R_{12} = -R_{21} \quad 3.3$$

$$R + T = 1 \quad 3.4$$

The behavior of waves in structures with more than one boundary is examined.

LATTICE FILTER REPRESENTATION

The problem taken up in this section is: what is the impulse response of a structure consisting of an arbitrary number of plane layers of known acoustic impedance, when the input is an ultrasonic plane wave. In Figure 3.2 a few wave paths are shown for a structure consisting of only three layers. The paths are represented for clarity by slanted lines, although in reality they are normal to the layer boundaries. A simple convention for labeling those paths is introduced here. A three digit number is associated with each path, where the first digit represents the number of transits of the first layer, the second digit the same quantity for the second layer and so on. It is obvious that even for



$$R_{12} = -R_{21}$$

$$R_{12} + T_{12} = R_{21} + T_{21} = 1$$

Figure 3.1 REFLECTION AND TRANSMISSION ACROSS A BOUNDARY

FIRST ORDER ARRIVALS

	AMPLITUDE	DELAY
A	c_0	0
B	$c_1(1 - c_0^2)$	τ_1
C	$c_2(1 - c_1^2)(1 - c_0^2)$	$\tau_1 + \tau_2$

SECOND ORDER ARRIVALS

	AMPLITUDE	DELAY
A	$c_0 c_1^2(1 - c_0^2)$	$2\tau_1$
B	$c_0 c_2^2(1 - c_1^2)^2(1 - c_0^2)$	$2(\tau_1 + \tau_2)$
C	$c_1^2 c_0 c_2(1 - c_1^2)(1 - c_0^2)$	$2\tau_1 + \tau_2$

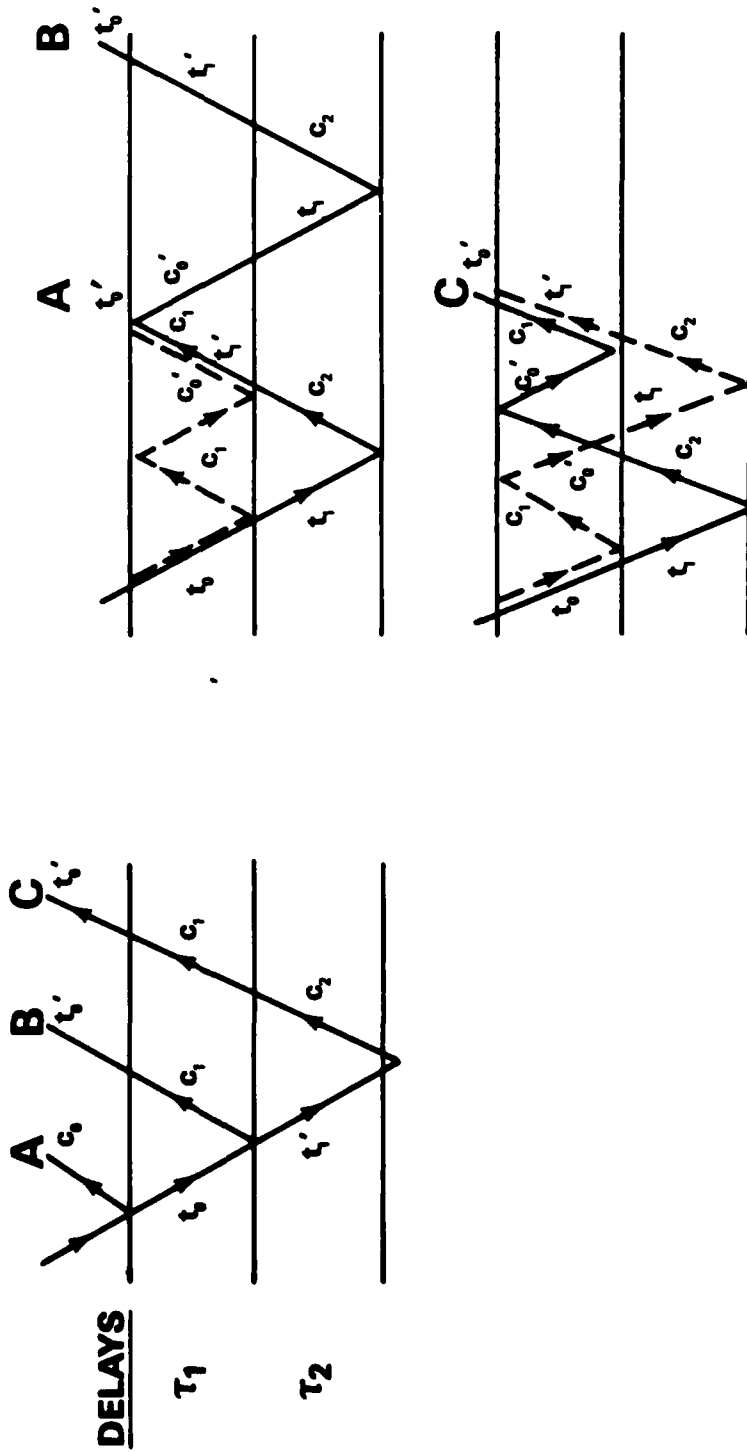


Figure 3.2 RAY TRACING FOR A TWO LAYERED STRUCTURE

such a simple structure, there are a great number of arrivals, and that some systematic method is required to keep track of their amplitudes and arrival times.

Such a method has been developed by Robinson and Trietel [3] and will be followed here. Figure 3.3 shows the k and $(k+1)$ th layers of a structure. The reflection coefficient for downgoing wave at their boundary is denoted by R_k , and the downgoing transmission coefficient by T_k . The equivalent upward going coefficients are denoted by primes. The two way transit time in a layer is equal to twice the thickness of the layer divided by the velocity of the ultrasonic pulse in the layer, and this will be denoted τ_k for the k th layer.

Two waves exist in each layer - an upward going and a downward going wave. Their amplitudes as a function of time are denoted by $U_k(t)$ and $D_k(t)$, respectively.

The following equations relate the amplitudes of these waves at the tops of their respective layers. The inclusion of τ_k in the time argument accounts for the delay experienced by the wave in traveling from the top of the k th layer to the top of the $k+1$ th layer. Thus, these equations relate amplitudes at different times as well as in different positions.

$$U_k(t-\tau_k) = R_k D_k(t+\tau_k) + T'_k U_{k+1}(t) \quad 3.5$$

$$D_{k+1}(t) = T_k D_k(t+\tau_k) + R'_k U_{k+1}(t) \quad 3.6$$

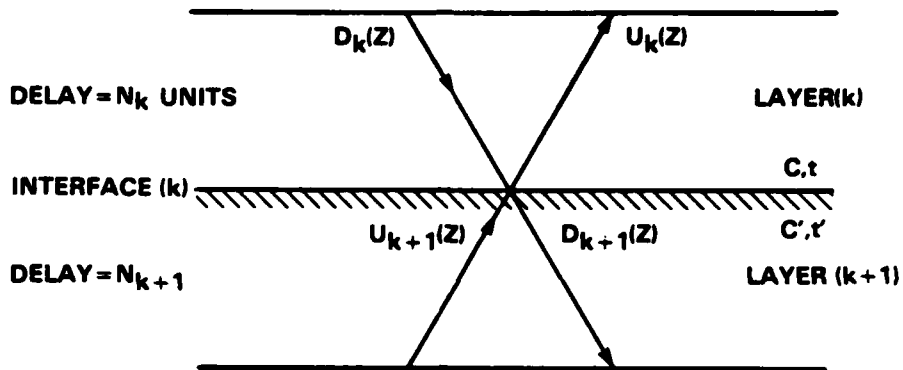
Using the facts that $R_k = -R'_k$ and that $T=1-R$, these equations become

$$U_k(t-\tau_k) = R_k D_k(t+\tau_k) + (1+R_k) U_{k+1}(t) \quad 3.7$$

$$D_{k+1}(t) = (1-R_k) D_k(t+\tau_k) - R_k U_{k+1}(t) \quad 3.8$$

The waveforms are inevitably sampled in time. For such waveforms the z transform notation forms a convenient representation[3]. The relevant properties of the z transform are that to find the transform of the sampled time series $f(n\Delta t)$, we form the sum over n of $z^n f(n)$. Then the z transform of $D(t)$ and $U(t)$ are denoted $D(z)$ and $U(z)$, and delays in time are represented by multiplication by z^n , where n is the time delay in units of the sampling time Δt . Therefore the equations 3.7 and 3.8 can be rewritten as

$$z^{N_k} U_k(z) = R_k z^{-N_k} D_k(z) + (1+R_k) U_{k+1}(z) \quad 3.9$$



$$\begin{bmatrix} D_k(z) \\ U_k(z) \end{bmatrix} = \frac{z^{N_k}}{1 - C_k} \begin{bmatrix} z^{-2N_k} & C_k z^{-2N_k} \\ C_k & 1 \end{bmatrix} \begin{bmatrix} D_{k+1}(z) \\ U_{k+1}(z) \end{bmatrix} = M_k \begin{bmatrix} D_{k+1}(z) \\ U_{k+1}(z) \end{bmatrix}$$

TO GET THE IMPULSE RESPONSE $U_k(z)$, SET $U_{k+1}(z) = 0$, $U_k(z) = 1$

Figure 3.3 WAVE EQUATION AT INTERFACE

$$D_{k+1}(z) = (1-R_k)z^{-N_k} D_k(z) - R_k U_{k+1}(z) \quad 3.10$$

where $N_k = \tau_r/\Delta t$.

These equations can in turn be rewritten in matrix form as

$$\begin{bmatrix} D_k(z) \\ U_k(z) \end{bmatrix} = \frac{N_k}{1+R_k} \begin{bmatrix} -2N_k & -2N_k \\ z & R_k z \\ R_k & 1 \end{bmatrix} \begin{bmatrix} D_{k+1}(z) \\ U_{k+1}(z) \end{bmatrix} \quad 3.11$$

The matrix equation is similar to a two port input-output lattice filter, as shown in Figure 3.4. The inputs terminals comprise the down- and up-going transforms in the k^{th} layer while the output terminal are the corresponding pair in the $(k+1)^{\text{st}}$ layer. For the simple case of a single interface, the solution is obtained by applying the boundary conditions. If a pulse is sent down in the k^{th} layer ($D_k(z)=1$) and the second layer is an infinite half-space ($U_{k+1}(z)=0$) then the pulse-echo response is

$$\frac{U_k(z)}{D_k(z)} = R_k$$

Similarly the through-transmission transfer function is

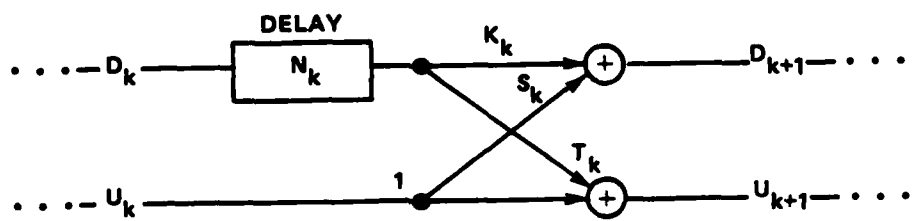
$$\frac{D_{k+1}(z)}{D_k(z)} = z^{N_k}$$

The former is the reflection coefficient while the latter represents a pure delay of N_k units.

The utility of equation 3.11 is that it may be used to represent the behavior of an arbitrary number of layers, by multiplying together the matrices for each layer. Thus the response at the top of the first layer, due to the wave in all M layers of a structure, is found from

$$\begin{bmatrix} D_0(z) \\ U_0(z) \end{bmatrix} = M_0 M_1 \dots M \begin{bmatrix} D_m(z) \\ U_m(z) \end{bmatrix} \quad 3.12$$

If we take the (M th) layer to be infinitely thick, the amplitude of the upgoing wave $U_m(z)$ is zero, since there is no reflector to direct energy upward. Furthermore, we may set the amplitude of the downgoing wave in the first layer, $D_1(z)$, equal to 1, and solve for the amplitude of the upgoing wave in the first layer, $U_1(z)$. This polynomial



CASE 1: NORMAL INCIDENT WAVE AND NON-ATTENUATIVE MEDIA

$$K_k = 1, S_k = -T_k = R_k \text{ THE REFLECTION COEFFICIENT}$$

Figure 3.4 LATTICE REPRESENTATION OF WAVE AT INTERFACE

represents the z transform of the impulse response of the layered structure, the desired quantity. All reflections and transmissions which return energy to the top of layer 1 are accounted for in $U_1(z)$.

SIMULATION FOR BRONZE-RUBBER STRUCTURE

The results obtained by the model for the structure shown in Figure 3.5 are discussed. This structure consists of layers of water, bronze, epoxy, rubber, epoxy, and bronze underlaid by an infinite halfspace of rubber. The dimensions, velocities and acoustic impedances are as shown in the accompanying table. The thickness of the rubber layer has been chosen such that its time delay is equal to the time delay in bronze.

Figure 3.6 shows the model impulse response. Time zero is taken to be the arrival of the pulse from the water-bronze interface, but this pulse has been suppressed in Figure 3.6, as it is of no interest for inspection.

This time domain waveform is not the z transform given by Equation 3.12, but is determined from that z transform by interpreting terms of the form $A_n z^n$ as pulses of amplitude A at time n (in units of Δt).

Each term in this waveform, which is called a reflection series, can be interpreted physically. The first arrival, labeled (100) in the notation of Figure 3.6, is a reflection from the first bronze-epoxy interface. It is negative because the impedance of bronze is greater than that of epoxy so the reflection coefficient is negative. A series of large arrivals, labeled 200, 300,.... continue throughout the reflection series, corresponding to reflected energy reverberations in the first bronze layer. Each is negative because the bronze layer is bounded on each side by acoustically "softer" materials; i.e., materials of lower acoustic impedance. Hence each arrival has undergone an odd number of reflections, each involving a negative reflection coefficient.

Following the 100 return is a negative pulse labeled 110. This pulse has been reflected once, from the bottom of the epoxy layer, where the reflection coefficient is negative because epoxy is harder than rubber. Its time delay with respect to the 100 return is equal to the time delay in the epoxy layer. After another epoxy time, a positive return appears. This energy has traversed the bronze layer once, and the epoxy layer twice, so it is labeled 120. It is positive because the reflection coefficient going from epoxy to bronze is positive, and this coefficient is multiplied by the square of the negative epoxy-rubber coefficient to arrive at the overall sign.

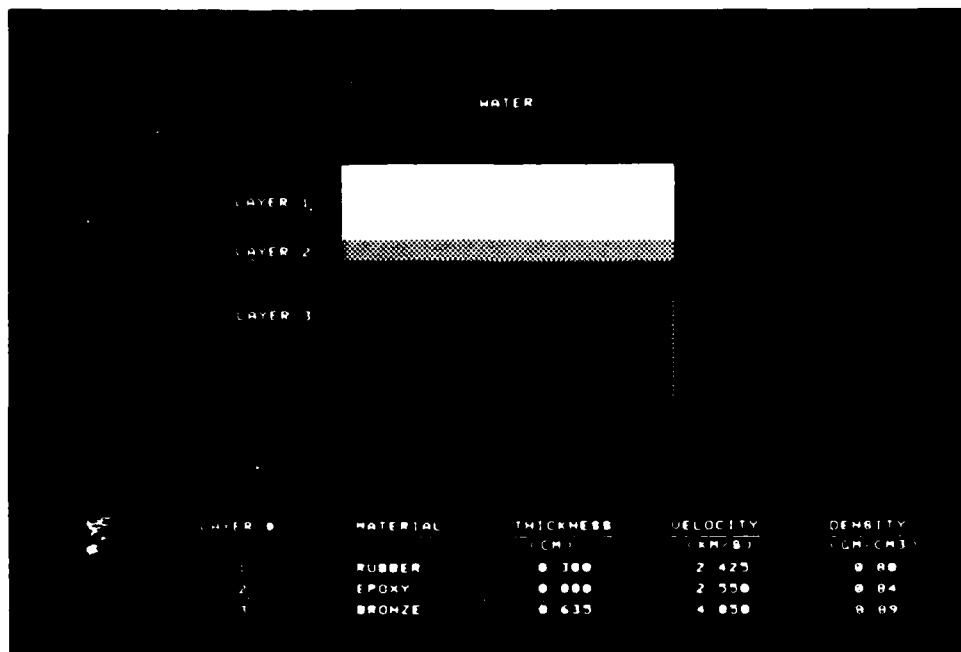


Figure 3.5 BRONZE-RUBBER MULTILAYER STRUCTURE

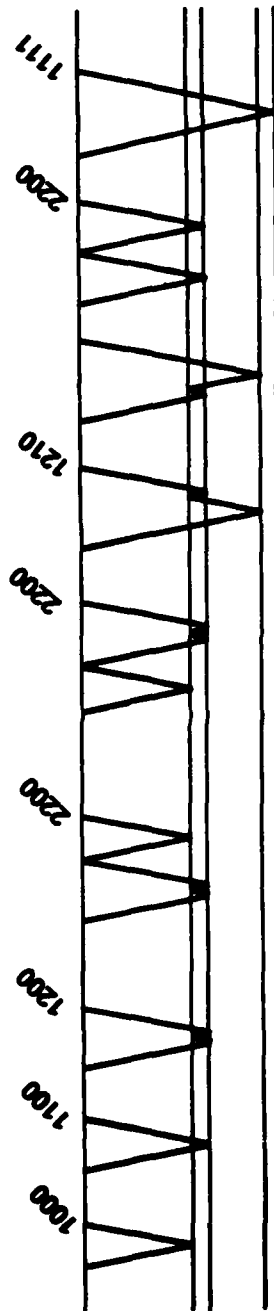
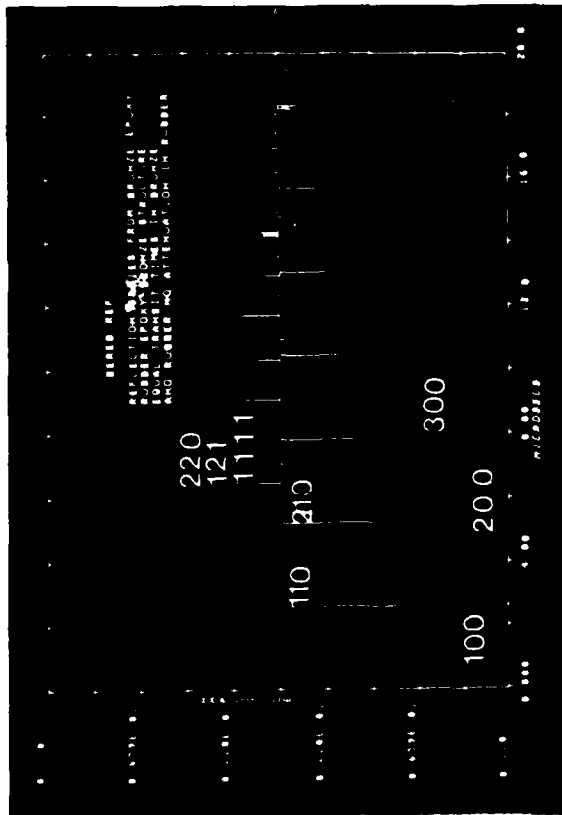


Figure 3.6 REFLECTION SERIES FROM GOOD SPECIMEN

Each term of the form $M00$, where M is the reverberation number, is followed by a similar series of returns, corresponding to M transits of the bronze layer, and one or more transits of the epoxy layer. However, these terms are not due to just one path. For example, there are three distinct paths which contribute to the single pulse labeled 210 and 111. One of these involves the ray which travels through the bronze, epoxy, and rubber layers, and is hence labeled 111. The fact that the bronze and rubber layers have the same time delay means that this path is of the same length in time as one which makes two transits of the first bronze layer and one of the epoxy layer, and is labeled 210. There are two such 210 paths; one which first goes to the bottom of the epoxy layer and then makes a single reverberation in the bronze layer, and a path in which a bronze layer reverberation is followed by a transit of the epoxy layer. The model takes all these paths into account, and predicts an amplitude equal to the algebraic sum of their amplitudes.

Other terms in the reflection series can be interpreted in a similar way. As time increases this becomes more difficult, because of the multiple paths associated with each arrival. Without the model developed here prediction of the reflection series would be a very difficult task.

The reflection series of Figure 3.6 is the impulse response, and will never be observed in a real situation. A more realistic response is that shown in Figure 3.8 where the reflection series of Figure 3.6 has been convolved with the transducer response shown in Figure 3.7. The transducer is centered at about 5 MHz, and is representative of those used in this work.

Even in the noise-free environment of Figure 3.8, it can be seen that the smaller returns are not resolved, but are interfered with by the bronze reverberations. A transducer with a much shorter response in time would be required to distinguish these returns from one another.

The situation will be worse when the effects of noise are added. Since the returns from the rubber layer are about 20 dB below those from the bronze layer, a signal to noise ratio of at least 20 dB is required to detect them, even if they were not interfered with by the bronze reverberations. This places a severe demand on the data collection and signal processing tasks involved.

INCORPORATION OF A FLAW IN MODEL

The model developed above can be used to predict the response of a layered structure containing a flaw, if the reflection and transmission coefficients associated with the flaw can be determined. A disbond at an interface can probably be modeled as a void in the epoxy. The acoustic impedance

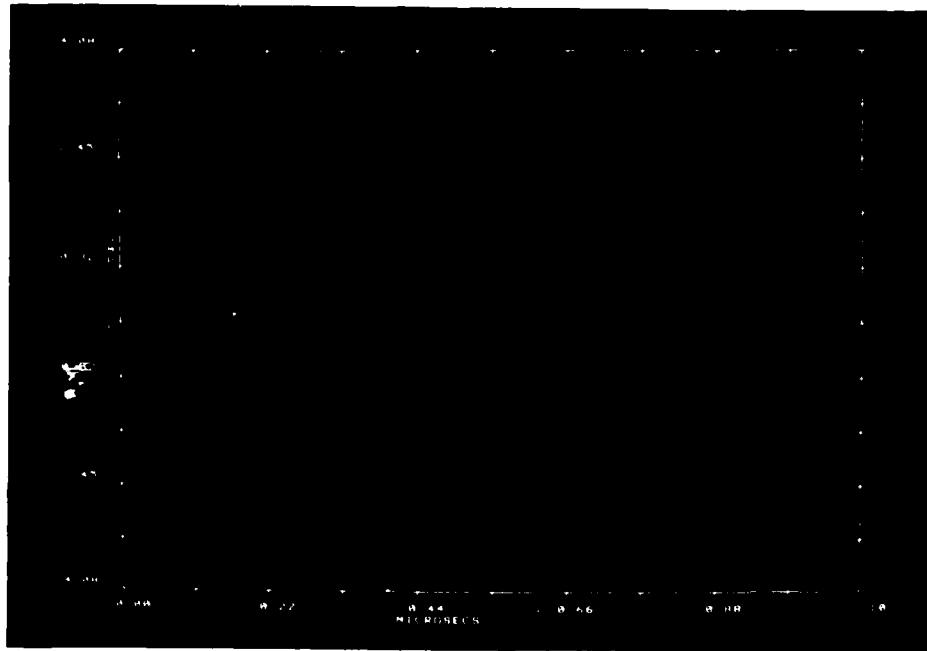


Figure 3.7 TRANSDUCER IMPULSE RESPONSE

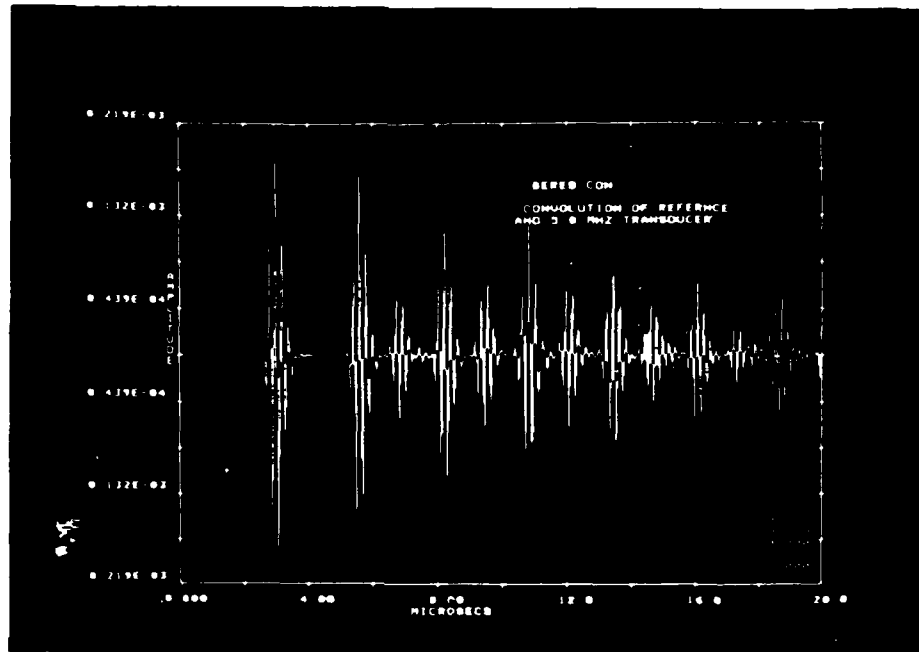


Figure 3.8 SIMULATED RESPONSE WITH 5.0 MHZ TRANSDUCER AND SNR=40 dB

of the void is virtually zero, so equation 3.1 for the reflection coefficient reduces to $R = -1$, whether the medium next to the void is bronze or rubber. Similarly, $T = 0$ in either case. By inserting these coefficients in the proper place in the model we can predict the response of the reflection series to a flaw.

This is done in Figures 3.9 and 3.10. In 3.9 the rubber at the bottom of the first bronze layer has been replaced by a void. Comparison with Figure 3.6 will show that the bronze reverberations die away at a lesser rate in the flawed case than when no flaw is present. This is because the transmission coefficient at the bottom of the bronze is zero in the flawed case, no energy can propagate downward into the rest of the structure, and this energy must appear in the bronze reverberation series. The returns corresponding to reverberations in rubber and in the second bronze layer are missing in Figure 3.9.

A flaw at the bottom of the rubber layer results in much more subtle changes, as shown in Figure 3.10. The dominant terms in the series, those due to the bronze reverberations, are unaffected by the flaw, which makes itself felt in terms such as the (110) response. This term in Figure 3.9 is somewhat larger than is the 110 term in Figure 3.6, due to the larger reflection coefficient in the flawed case. However, the effect is small, and would be difficult to detect when the presence of noise, and the effects of a real transducer were incorporated into Figure 3.10. If the time delay in the rubber were made equal to that in the bronze, as is the case in the structure of interest, the 200 arrival would interfere with the 110 arrival, completely masking the small change in the 110 term demonstrated in Figure 3.10. Hence, flaws at the bottom of the rubber layer (and deeper) are predicted to be quite difficult to detect ultrasonically.

EFFECTS OF ATTENUATION

So far, it has been assumed that ultrasonic energy travels from one side of a layer to the other without loss. This is a good approximation for many materials over short paths, but not for rubber in the thickness used here. Ultrasonic energy in rubber is highly damped, the damping increases with frequency. A constant Q model for the attenuation fits the data well.

A complete discussion of this model has been given by Knopoff [6]. It assumes that the medium is linear, and that the same fractional energy is lost per cycle, independent of frequency. Under these assumptions, the amplitude A of a plane wave of velocity v as a function of distance x is

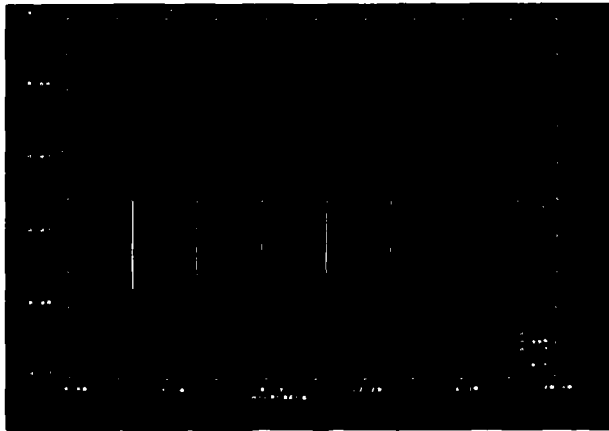


Figure 3.9 TOP OF RUBBER LAYER

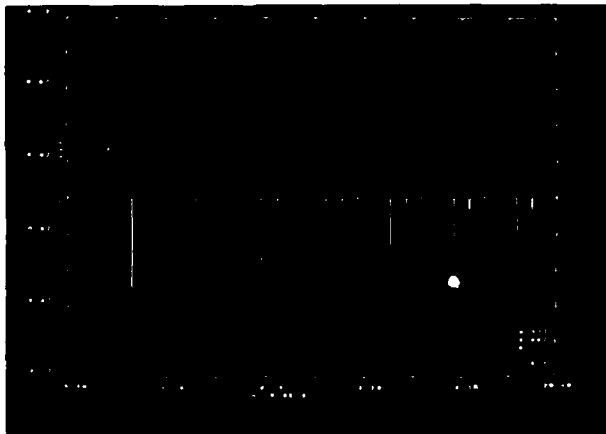


Figure 3.10 BOTTOM OF RUBBER LAYER

$$A(f,x) = A_0 \exp(-\pi fx/Qv) \quad 3.13$$

A is the initial amplitude at $x=0$, f is the frequency, and Q is a dimensionless constant dependent on the medium. Q is equal to π times the number of wavelengths of motion required to reduce the amplitude to $1/e$ of its initial value. Large values of Q correspond to low attenuation, and vice versa.

This model has been shown to be a good one for a wide variety of materials and a wide range of frequencies. Metals may display Q s of several hundred to thousand, while Q for unconsolidated soil may be only 10 or so.

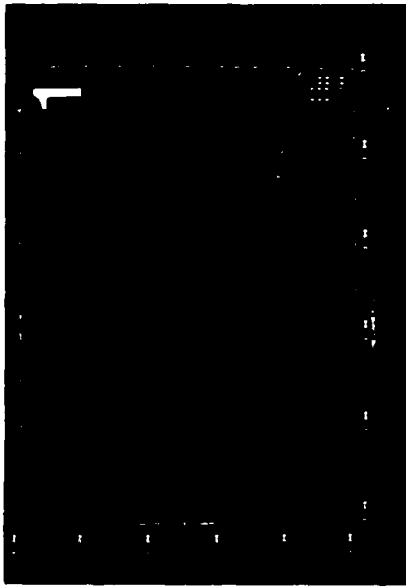
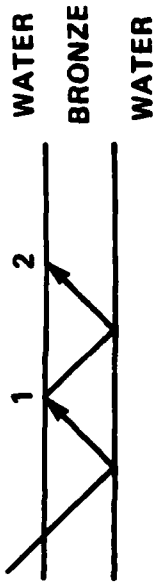
It is a straightforward matter to determine ultrasonic Q values experimentally. A sample, consisting of a plate of suitable thickness x and ultrasonic velocity v , is interrogated in pulse-echo mode. Multiple internal reverberations will be observed, as energy is reflected alternately from side to side within the plate. The spectra of these pulses are calculated in the usual way. According to equation 3.13, the difference between the logarithm of the n th pulse and that of the logarithm of the $(n + 1)$ st pulse is

$$\log A_n - \log A_{n+1} = C - (\pi fx/Qv) \quad 3.14$$

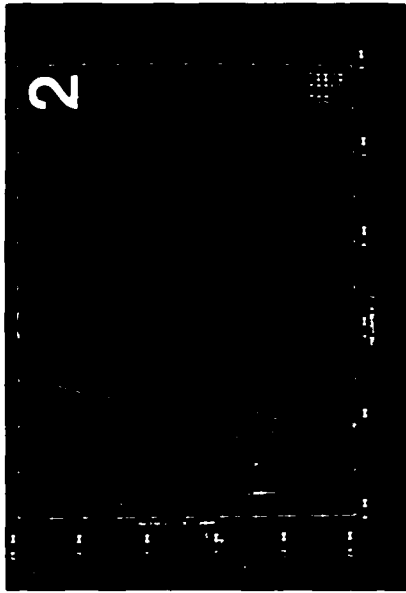
where C is a constant which depends on the reflection coefficients at the front and back surfaces, but not on the frequency. Hence, if we plot the difference in the log spectra as a function of frequency, and fit a straight line through these data, its slope will be $-\pi x/Qv$. From this slope Q can be easily determined.

This experiment was performed for both bronze and rubber samples, with the results shown in Figures 3.11 and 3.12. In Figure 3.11, successive back surface log spectra, and their difference, are shown for bronze. Over the frequency interval from about 4 to 10 MHz the difference of the logarithms is virtually constant. Outside this band there is not enough power to reliably measure the spectral values, and differences in the log spectra are not significant. Since the slope of the log spectral difference is zero, we infer that Q in bronze is infinitely high, at least within the spectral range and accuracy of this measurement.

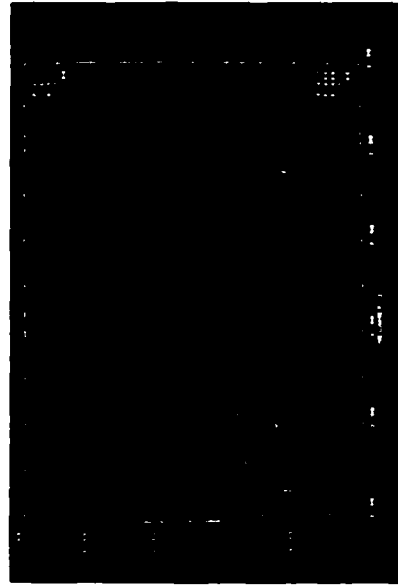
The results for rubber are shown in Figure 3.12. Here the usual bandwidth extends only to about 7.5 MHz, due to high frequency attenuation in rubber. The slope of the log



FIRST BACK SURFACE SPECTRUM



SECOND BACK SURFACE SPECTRUM

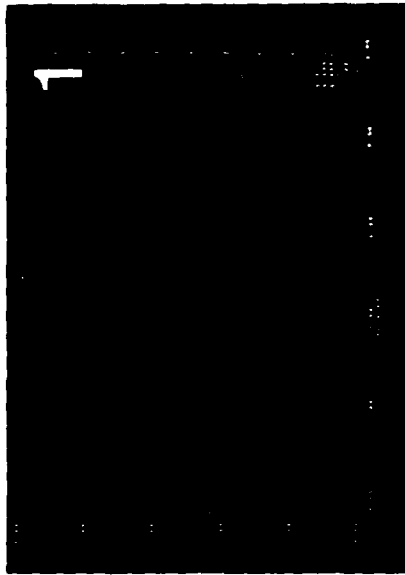
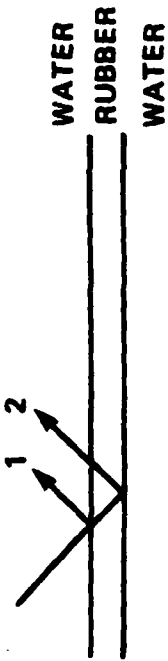


FIRST BACK SURFACE AND DIFFERENCE OF LOG SPECTRA (DOTTED)

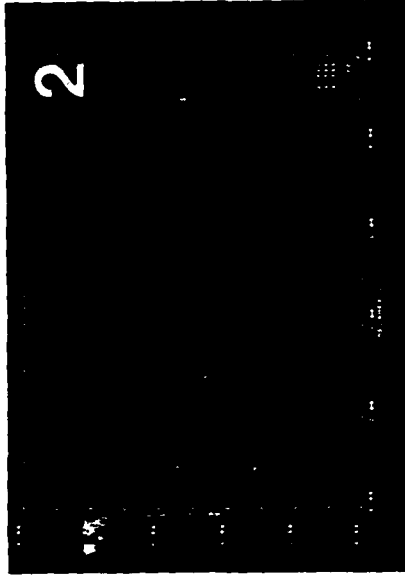
0 —→ ∞

ATTENUATION AT 5 MHZ \approx 0 dB/MM

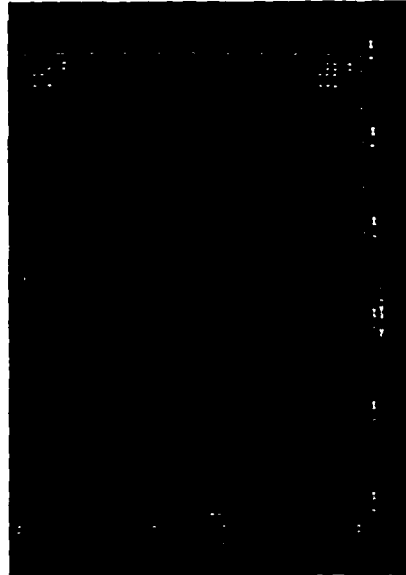
Figure 3.11 ATTENUATION IN BRONZE



FRONT SURFACE SPECTRUM



BACK SURFACE SPECTRUM



FRONT SURFACE SPECTRUM
AND DIFFERENCE OF LOG SPECTRA (DOTTED)

SLOPE OF DIFFERENCE SPECTRA ≈ 4.1 dB/MHZ
 $Q \approx 9$
 AT 5 MHZ ATTENUATION IN RUBBER = 6.2 dB/MM

Figure 3.12 ATTENUATION IN RUBBER

difference spectrum is about 4.1 dB/MHz, which corresponds to a Q of about 9. This rubber is therefore highly attenuative, and we expect little energy to travel through the rubber layers, whereas bronze attenuation is negligible.

For a narrow band signal we can calculate attenuation, in dB/mm, valid at the center frequency of the transducer. This value will be adequate to calculate the effect of attenuation on peak amplitudes. To do so, we use $Q = 9$, $x = 1$ mm, and $f = f_0$, the center frequency of the transducer, in equation 3.13, and express the fractional reduction in amplitude in dB. The attenuation in rubber at 5 MHz calculated in this way is 6.2 dB/mm.

Since frequency dependent attenuation actually affects different frequency components differently, the shape of a wide band pulse changes as it propagates through an attenuative medium. To calculate a time domain operator to account for this effect, the treatment of Kak & Dines [7] is followed. Defining an attenuation coefficient such that

$$\alpha = \frac{\pi x}{Qv} \quad 3.15$$

so that the expression for attenuation becomes

$$A = A_0 e^{-\alpha f} \quad 3.16$$

the transfer function of a layer is represented by

$$H(f) = e^{-\alpha f - i2\pi f x/v} \quad 3.17$$

where the symbols have their usual meanings. The first term is due to attenuation and the second is a lossless form and is simply a phase shift. This transfer function relates the signal at the top of a layer to that at the bottom through

$$R(f) = I(f) H(f) \quad 3.18$$

where R and I are the signals at the bottom and top of the layer, respectively. In the time domain, we have

$$r(t) = \int_{-\infty}^t i(\tau) h(t-\tau) d\tau \quad 3.19$$

where R, I and H are Fourier transforms of r, i and h. Then the expression for h(t) is

$$h(t) = \int_{-\infty}^{\infty} H(f) e^{i2\pi ft} df \quad 3.20$$

$$= \frac{\frac{\alpha}{2\pi^2}}{(\alpha/2\pi)^2 + (t-x/v)^2} \quad 3.21$$

For data sampled at an interval Δt , this becomes

$$h(n\Delta t) = \frac{\frac{\alpha}{2\pi^2}}{(\alpha/2\pi)^2 + (n\Delta t - x/v)^2} \quad 3.22$$

and its z transform may be written as

$$H(z) = \sum_{n=-\infty}^{\infty} \frac{\frac{\alpha}{2\pi^2}}{(\alpha/2\pi)^2 + (n - x/v)} \cdot z^N$$

By a change of variables to $m = n + N$, where $N = x/v$ the time delay in the layer, the definition $p = \alpha/2\pi$ and some manipulation, we have

$$H(z) = \frac{z^N}{\pi p} \sum_{m=-\infty}^{\infty} \frac{z^m}{1 + (m^2/p^2)} \quad 3.24$$

The term z^N represents the time delay involved in traversing the layer, and the rest of $H(z)$ represents the effect of attenuation.

For evaluation, the sum in equation 3.24 must be truncated at some reasonable value, say when the amplitude of the terms in the sum has dropped to 1/10 their value at $m = 0$. Then we have

$$H(z) = \frac{z^N}{\pi p} \sum_{m=-M_k}^{M_k} z^m / (1+m^2/p^2) \quad 3.25$$

where $M_k = 3p$

The effects of $H(z)$ are twofold; first, a reduction in peak amplitude by a factor of p , and second a broadening of the incident pulse. The amount of broadening will depend on the form of the pulse, but for an impulse, the full width at half maximum will be $2p$. The broadening extends in both directions in time, so the signal is no longer causal. This effect is not physical, and is the result of the fact that any model for attenuation which involves a Q which is constant down to the lowest frequencies is inherently non causal. As a practical matter the limitations on signal bandwidth imposed by a real transducer will make real signals causal after convolution with the operator $A(f)$. Futterman [8] gives a good discussion of this point.

We may now write equation 3.11 as

$$\begin{bmatrix} D_k(z) \\ U_k(z) \end{bmatrix} = \frac{N_k}{1-R_k} \begin{bmatrix} H(z) \cdot z^{-2N_k} & R_k H(z) z^{-2N_k} \\ R_k & 1 \end{bmatrix} \begin{bmatrix} D_{k+1}(z) \\ U_{k+1}(z) \end{bmatrix} \quad 3.26$$

here $H(z)$ is defined in equation 3.25.

This is the explicit expression for including the effects of attenuation with constant Q into the model developed previously. To extend it to the case of several layers, we need only put subscripts on M , p and N to refer to the appropriate layer, and multiply matrices together as before.

PROPAGATION AT OFF-NORMAL INCIDENCE

The development presented in the preceding chapters refers to the case of normal incidence only. However, it can be modified to account for the case where the ultrasonic energy is incident at any angle from the normal in a straight-forward way. For such off-normal incidence several new effects occur, among them the presence of mode converted energy in solids. That is, at angles other than zero, energy is converted from shear to compressional waves and vice versa, when a wave strikes a boundary.

The analysis presented here will not be complete, in that not all modes will be accounted for. However, it will be seen that the neglected modes are unimportant in this application. A later effort will consider the case where amplitudes of all possible modes are required.

The development of the matrix formulation of the arrival times and amplitudes presented above did not depend explicitly on normal incidence. All that was assumed was a reflection and transmission coefficient at each boundary, and a time delay within each layer. These quantities take on particularly simple forms for the normal incidence case, but they can be calculated for the off-normal incidence case and can be included in the model as before.

To illustrate this point, refer to Figure 3.13. A wave propagates downward through medium 1, and is reflected and transmitted at an interface. Wave paths are now drawn in their correct relation to boundaries. For the moment we ignore mode conversion. For off-normal incidence, the travel path in each layer is found by dividing the path length for normal incidence by the cosine of the angle with respect to the normal, of the sound beam in that layer as shown in Figure 3.13. It follows that the normal incidence time delay is also divided by the cosine of the angles for off-normal incidence. Insertion of this corrected time delay in Equations 3.5 and 3.6 leads to the correct predicted time delay for any multiply reflected wave.

The reflection and transmission coefficients of Equations 3.1 and 3.2 are also modified for the off-normal incidence case. Three important effects are present for the case where two solids abut one another. First, at most angles a wave incident on the boundary in one medium will give rise to two waves in that medium, and two waves in the medium on the far side of the boundary. These waves are required for solid-solid boundaries to satisfy the conditions of continuity of displacement and stress everywhere.

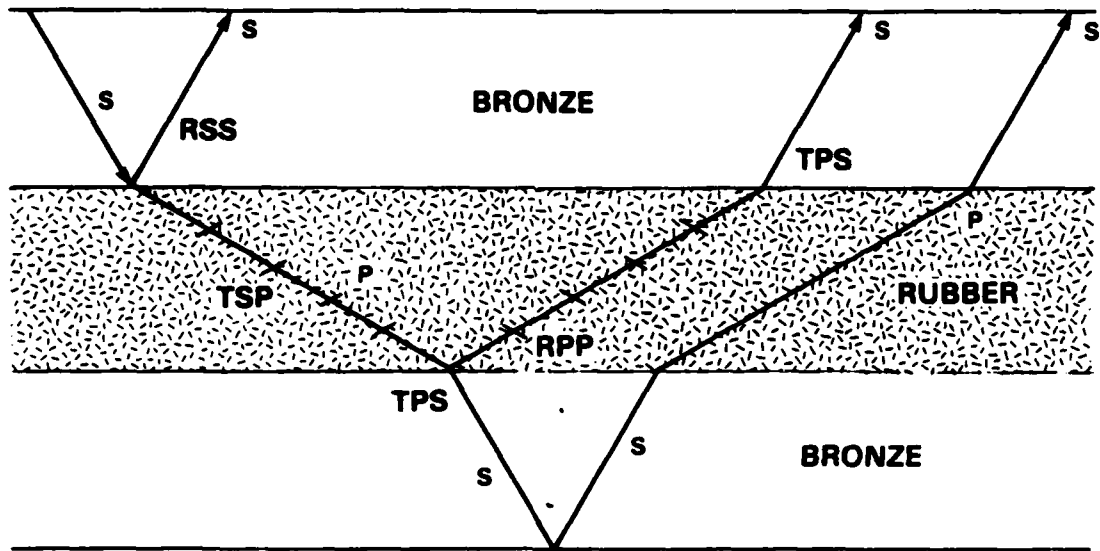


Figure 3.13 ANGLE BEAM INSPECTION

Second, over certain angular ranges, some of the reflected waves do not propagate into either medium, but are confined to the boundary between media. They are never detected by a transducer on the surface, but carry energy away from the interface, and must be considered in order to correctly predict the amplitudes at the surface.

Finally, over the range where the waves referred to above are confined to the boundary, the reflection and transmission coefficients are complex. This means that each frequency component of the incident wave suffers a time delay upon reflection or transmission, and this delay is frequency dependent. The emerging pulse (if a pulse is incident, as is usually the case) is dispersed, and this must be accounted for when amplitudes are calculated.

The above simple theory, which accounts for only one wave in each medium, may be used when in fact two waves are actually present in each. First some notations are introduced. Compressional waves not converted to shear waves, but remain compressional waves, are denoted as R_{pp} . Here the conventional seismic notation p for compressional waves and s for shear waves is used. Where mode conversion to shear waves takes place, the reflection coefficient is denoted by R_{ps} . Similarly, reflection without mode conversion for an incident shear wave is associated with a reflection coefficient R_{ss} and that with mode conversion to p waves with R_{sp} . Transmission coefficients T are assigned the same notation. Thus T_{sp} refers to the amplitude of a wave which undergoes conversion from an s wave to a p wave as it crosses a boundary, and so on.

If we calculate correctly all 8 coefficients at each boundary (four for downgoing waves and four for upgoing waves), and pick which wave to keep track of in each layer (the theory can handle only one per layer) the proper coefficients to use in Equation 3.11 can be selected to predict the amplitudes of these waves. For example, suppose the interest is in shear wave in layer 1 and compressional wave in layer 2: Then R_{ss} and T_{sp} for waves traveling downward from layer 1 to layer 2 are needed. Waves corresponding to R_{sp} , and to T_{ss} exist, but will be ignored. The coefficient R_{pp} and T_{ps} for waves traveling upward in the second layer are also needed. Again the waves related to two other coefficients are ignored. With these coefficients, and the modified time delays in each layer, Equation 3.11 can be used to predict amplitudes and times of arrival in this twolayered structure which consist of shear waves in the first layer and compressional waves in the second.

This example is not so unrealistic as it might seem at first. If the angle in the first layer, which is bronze, is selected beyond the critical angle, there will be no compressional wave in the bronze. The energy corresponding to the compressional wave will propagate along the boundary, as discussed above. Therefore there is no contribution to the reflection series from the term R_{sp} , and nothing is lost by ignoring it.

Further, a great deal of experimental evidence indicates that shear waves in rubber are highly damped, so that they are not observed in the reflection series for reasonable thicknesses of rubber. The energy represented by terms such as T_{ss} , corresponding to shear waves in rubber generated by shear waves in bronze, is lost to heat. It must be accounted for when calculating the other reflection and transmission coefficients, but once this is done, its contribution to the reflection series is negligible.

Therefore the model developed above is appropriate to the problem of alternate bronze and rubber layers. It can be extended to the case of several layers in the same way as was done for the case of normal incidence.

One effect not predicted by the model is the location of the emerging pulse of energy. For the normal incidence case, this point is just the entrance point, but for beams at an angle the emergence point is displaced by some amount. This distance can readily be calculated: it is just twice the layer thickness times the sine of the angle the relevant ray path makes with the normal. Each transit of each layer contributes this quantity to the overall displacement of the exit point, and therefore the contributions of all transits of all layers must be added to get the total displacement.

The angle of the ray path is generally different from layer to layer, and from mode to mode within a layer. It can be calculated by Snell's law. If θ_i is the angle made by the ray in question with respect to the normal, and v_i the velocity of the phase in the i -th layer, then

$$V = v_i / \sin(\theta_i) \qquad 3.26$$

holds for all layers. V is called the phase velocity, and is a constant throughout the layered structure.

Having found the formalism by which the arrival times and amplitudes may be calculated for the off-normal incidence case, the reflection and transmission coefficients referred to above are calculated. In [4] the potentials ϕ and ψ are introduced whose derivatives give rise to compressional and shear waves as follows:

$$\begin{aligned} u &= \partial\phi/\partial x - \partial\psi/\partial z \\ w &= \partial\phi/\partial z + \partial\psi/\partial x \end{aligned} \quad 3.27$$

where u and w are displacements in x and z , respectively.

The equations for continuity of displacement and stress at the boundary take the form

$$\begin{aligned} A_1 + A_1' &= M_{13} A_2 + M_{14} B_2 \\ B_1 - B_1' &= M_{23} A_2 + M_{24} B_2 \\ A_1 - A_1' &= M_{33} A_2 + M_{34} B_2 \\ B_1 + B_1' &= M_{43} A_2 + M_{44} B_2 \end{aligned} \quad 3.28$$

Here A refers to the amplitude of the compressional potential and B to that of the shear potential. The subscript 1 refers to the upper layer, and 2 to the lower layer. Reflected waves (present in the upper layer only) are denoted by a prime sign ('). The coefficients M_{ij} are functions of the material properties only, and are detailed in [4].

Only one incident wave at a time need be considered in the upper layer. In the case above, only a shear wave is incident there. Then the incident p wave amplitude A_1 is zero, and B_1 is the amplitude of the incident wave potential. We divide each of the Equations 3.28 by B_1 , and make the following identifications:

$$\begin{aligned} A_1'/B_1 &= R_{sp} \\ A_2/B_1 &= T_{sp} \\ B_1'/B_1 &= R_{ss} \\ B_2/B_1 &= T_{ss} \end{aligned}$$

Then the equations 3.28 can be written in matrix notation as

$$\begin{bmatrix} 0 \\ 1 \\ 0 \\ 1 \end{bmatrix} = \begin{bmatrix} -1 & 0 & M_{13} & M_{14} \\ 0 & 1 & M_{23} & M_{24} \\ 1 & 0 & M_{33} & M_{34} \\ 0 & -1 & M_{43} & M_{44} \end{bmatrix} \begin{bmatrix} R_{sp} \\ R_{ss} \\ T_{sp} \\ T_{ss} \end{bmatrix} \quad 3.30$$

Denoting the square matrix of coefficients on the right by H, the solution for the desired reflection and transmission coefficients is

$$\begin{bmatrix} R_{sp} \\ R_{ss} \\ T_{sp} \\ T_{ss} \end{bmatrix} = H^{-1} \begin{bmatrix} 0 \\ 1 \\ 0 \\ 1 \end{bmatrix} \quad 3.31$$

A complex matrix inversion routine is required to evaluate this expression on a digital computer.

Finally, to get amplitudes, the coefficients given above must be multiplied by $i\omega/v$ in accordance with equation 3.27. For the remainder of this report it is assumed that this has been done, and refer to T and R as amplitude transmission and reflection coefficients.

Figure 3.14 shows the theoretical reflection coefficients for the case of a shear wave in bronze incident on a rubber half space, as a function of the shear wave angle in bronze. Amplitudes are shown in 3.14a, and the phase in Figure 3.14b.

Figure 3.14a does not give all the information required to pick the optimum inspection angle. This is because the phase shift given in Figure 3.13b also affects the amplitude in the time domain. To see how it does so, take the incident pulse to be an impulse, given in the time domain by

$$\delta(t) = \int_{-\infty}^{\infty} e^{i\omega t} d\omega \quad 3.32$$

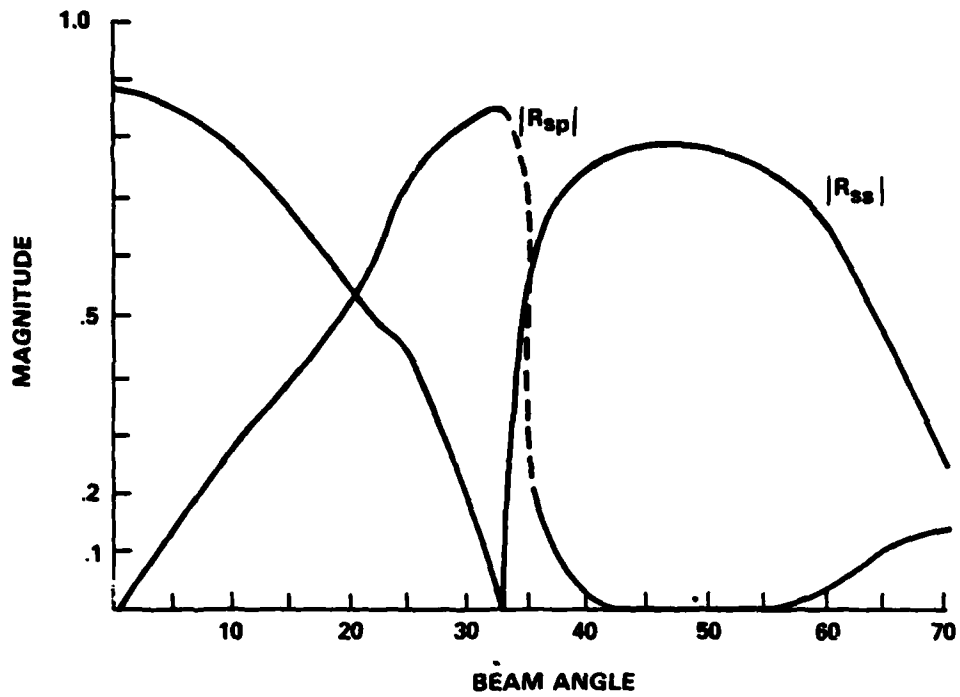
Then a reflected pulse $f(t)$, where the reflection coefficient is $r e^{i\theta}$, is given by

$$f(t) = r \int_{-\infty}^{\infty} e^{i\omega(t + \frac{\theta}{|\omega|})} d\omega \quad 3.33$$

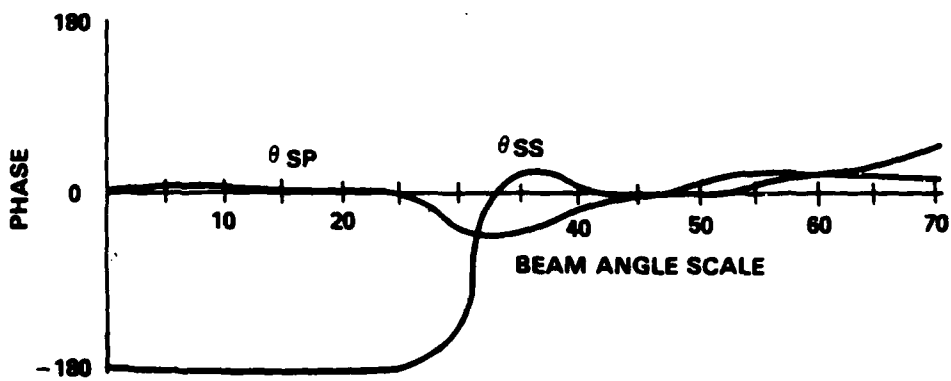
The presence of the absolute value of the frequency in the integral is required to make the phase shift correspond to an increase in the time for negative as well as positive frequencies.

This integral can be evaluated, and the resultant pulse is

$$f(t) = r\delta(t) \cos \theta + (r/2\pi^2 t) \sin \theta \quad 3.34$$



MAGNITUDE OF R_{sp} AND R_{ss} VERSUS ANGLE IN BRONZE



PHASE OF R_{sp} AND R_{ss} VERSUS ANGLE IN BRONZE

Figure 3.14 REFLECTION COEFFICIENTS BRONZE RUBBER INTERFACE

It is plotted in Figure 3.15 for several values of phase shift.

This pulse displays noncausal behavior in that it has non-zero amplitude at large negative times, but this is not cause for concern, for the same reasons that it was not in the case of the constant Q model. We have also made the assumption of plane wave behavior everywhere, and this is violated at low enough frequency (and hence large enough wavelength) for any finite size reflector.

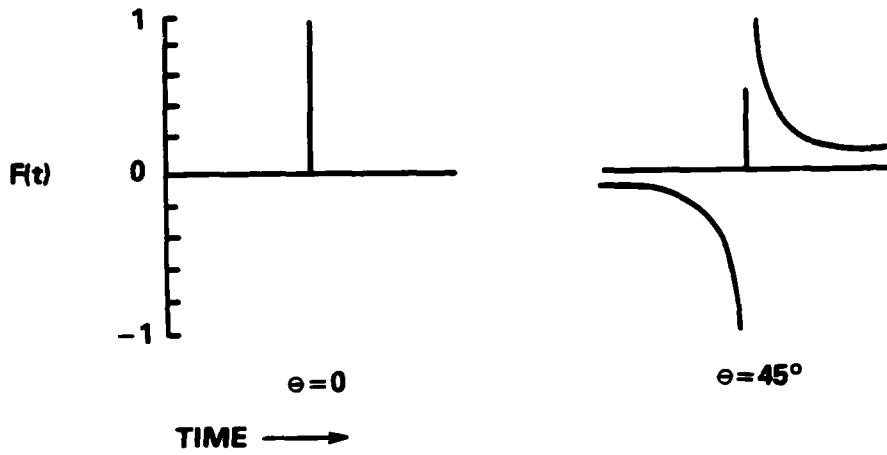
The general properties predicted for $f(t)$ by equation 3.34 have been verified seismically by Ewing, Jardetsky, and Press [4].

The utility of Equation 3.34 is that it may be convolved with the assumed shape of the incident pulse to find the time domain amplitude of the reflected or transmitted pulse. The peak amplitude of this pulse is what is really used for detection.

A reflection series for the structure of bronze and rubber referred to above is shown in Figure 3.16. It can be seen that the general effect of phase shifts in the terms of the reflection series is to broaden and reduce in amplitude the emergent pulse, an effect not favorable for detection. Hence a phase shift of zero is desirable in the return chosen for inspection of a particular layer.

The phase shift in any term of the reflection series is the sum of the phase shifts which that pulse has undergone during its passage from the sending to receiving transducer, so examination of the complete reflection series is required to pick a favorable angle. The search for the best angle of inspection is made tedious by the requirement to generate the reflection series at each angle, and convolve it with the transducer.

An angle of 20 degrees incident in water in bronze appears to be the most favorable angle for inspecting the bottom of the rubber layer. Although in general we want a large amplitude from the region under inspection, this is only part of the requirement. We would also like that amplitude to undergo a large change when a defect is present. That is, we want the response to be sensitive to the presence of a defect. Determining the sensitivity involves making two calculations, the first with the boundary as it would be without a defect, and the second with the defect present.



FOR A δ FUNCTION INPUT OUTPUT IS $f(t) = \cos \theta \delta(t) + \sin \theta / 2\pi^2 t$

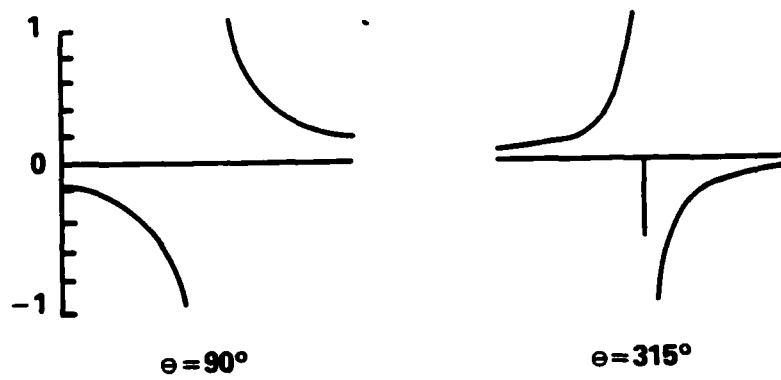
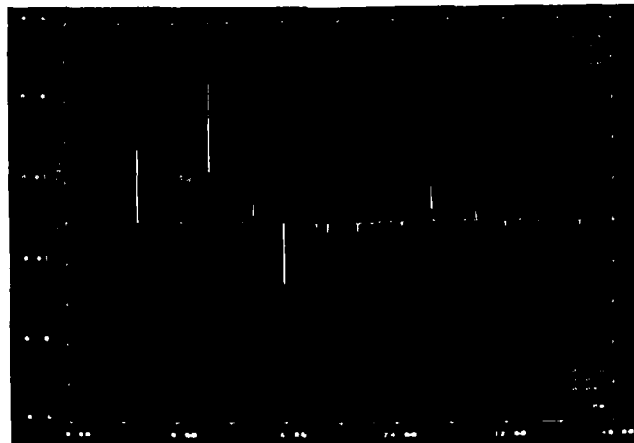
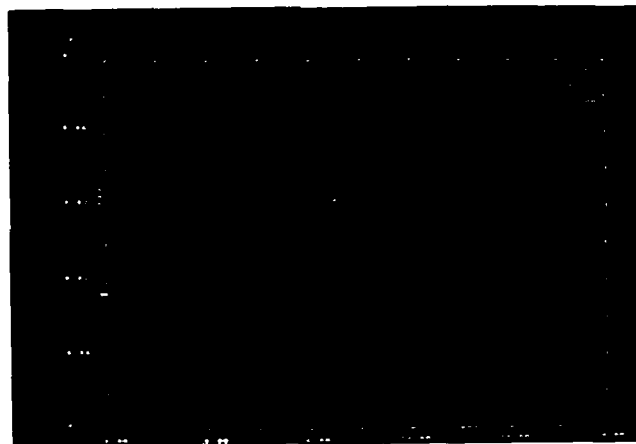


Figure 3.15 EFFECT OF PHASE SHIFT ON WAVEFORM



REAL & IMAGINARY PARTS



IMPULSE RESPONSE

Figure 3.16 EFFECT OF PHASE SHIFT IN ANGLED BEAM IMPULSE RESPONSE

The best circumstance would be that the boundary of interest gave rise to a large response without a defect, and another still larger response in the presence of a defect. This is not likely, and it is more probable that either the defect free response, or the defect-present response, will be undetectable. Acceptance of the absence of a response as indicating something about the boundary under inspection amounts to acceptance of negative evidence - drawing a conclusion from something which has not been observed. In the case where the defect free response is too small to observe, it can lead to a false dismissal. That is, the operator might assume that because he saw no return, the boundary was sound, whereas actually it was defective and some other problem interfered with the signal from the defect. Similarly, if the defect response is too small to observe, false alarms are possible, when the signal from a sound region is obscured by some unaccounted for effect. Since the choice of angle and which return to examine, is under the operators control, one may be able to decide which of these alternatives to accept. At this point an evaluation of the risks of each, beyond the scope of this work, is required.

ULTRASONIC DATA COLLECTION

INTRODUCTION

Ultrasonic data were collected from bronze-rubber specimens in water-immersion and contact-testing modes. Most of the data were collected using a 5 MHz transducer and in pulse-echo configuration. To insure repeatability of experiments several "header" parameters were recorded with each waveform which related to the instrumentation, experimental conditions, specimen description, A/D converter specifications and other observable conditions. The waveforms were recorded on a desktop computer at White Oak, Maryland and later analyzed at Tetra Tech's facility in Arlington, Virginia. Towards the end of the first phase of the project, telephone modem link and appropriate computer software have been developed at Tetra Tech to effect real-time data transfer in the future.

BRONZE-RUBBER SPECIMENS

Each sample multilayered specimen was 4" by 6" in surface dimensions. The bronze and rubber thicknesses were, respectively, 0.6350 and 0.3175 cm. These were designed specifically so that an acoustic wave would have approximately equal transit times, i.e., the acoustic velocity in bronze is nominally twice that in rubber. The rubber was available under the trade name DEADBEAT. The rubber-bronze layers were sealed with an epoxy whose trade name was ELASTOLOCK. The epoxy thickness in the specimens varied from 0.080 to 0.003 cm, however it was not uniform over the surface contact area. Although there were no samples with an intentional flaw, some specimens had incomplete epoxy contact between rubber and bronze. The bronze surface was machine finished while the rubber surface was sufficiently rough. A photograph of a sample specimen is shown in Figure 4.1.

Ultrasonic data were collected at five positions from most specimens: these were identified in the header in each waveform as the center position and north east, west and south positions. The directions were identified with respect to a specimen number inscribed in the northeast sector. A depiction of this nomenclature appears in Figure 4.2. Data were also collected from rubber and bronze specimens individually to determine material attenuation, reflection coefficient at the interfaces and phase velocity.



Figure 4.1 BRONZE RUBBER MULTILAYERED SPECIMEN

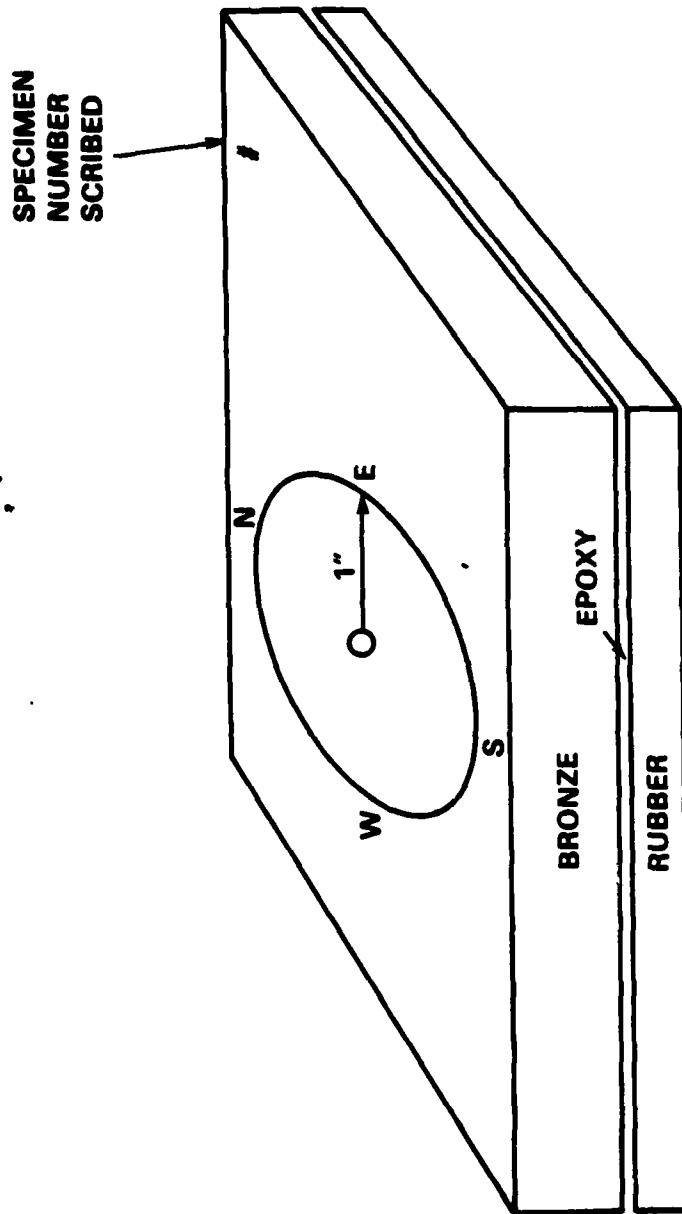


Figure 4.2 POSITIONS WHERE ULTRASONIC DATA WERE RECORDED

APPARATUS AND ULTRASONIC DATA COLLECTION

Figure 4.3 shows a schematic of the data flow from collection to acquisition and finally to data transfer and processing at Tetra Tech. Data collection was performed with specimen immersed in a water tank. The transducer, also immersed, could be moved in three axes to obtain normal incidence to specimen. An MP-101, MetroTek pulser-receiver was used to amplify the return signal, which could be displayed on a T7854 Tektronix oscilloscope. This was also a data acquisition unit and had a 10 bit dynamic range and 1024-words of memory. The sampling rate was adjustable and for the experiments was set at 51.2 MHz, i.e., ten (10) times the center frequency of the transducer. The time-bandwidth product of the A/D unit was fixed, at 512, however, i.e., increasing sampling rate would cause a decrease in window duration and vice-versa. The data were then transferred to cassette tapes on an HP-9825 minicomputer from the recorder buffer memory. These data could be plotted on a HP graphics plotter for data verification. Each data waveform received was preceded by "header information" relating to instrument settings, offsets in the data trace, sampling interval and attenuation setting on receiver amplifier. Along with this header information, a "header sheet" was prepared manually to completely describe experimental conditions for future repeatability. A sample header sheet is shown in Figure 4.4.

To insure full utilization of the 10 bit dynamic range, the signals were adjusted so that the first return from the material occupied full scale. This meant that the front surface return was always saturated and only served as a timing indicator. Usually the time delay on the oscilloscope was set so as to adjust data window at approximately the start of the front surface return. The recorder buffer memory was able to collect 1024 words of information; at a 51.2 MHz sampling rate, the data window was therefore 20 μ s long ($= 1/51.2 \times 1024 \mu$ s). In order to capture more data, a time delay of 20 μ s was added to the scope trace and then an additional 1024 words of data recorded. These data in the latter window were of smaller amplitude and required increasing the gain on the receiver amplifier. This two step procedure ensured a 40 μ s data window recorded in two steps, or approximately equivalent to 13 transits in the first bronze layer (bronze transit time: $2 \times 6.35/4.85 = 3.0 \mu$ s).

The pulser was usually set at maximum allowable damping for the broadest signal bandwidth. This meant reduced energy into the material; sometimes a compromise had to be made. The receiver gain could also be adjusted for overall maximum dynamic range utilization.

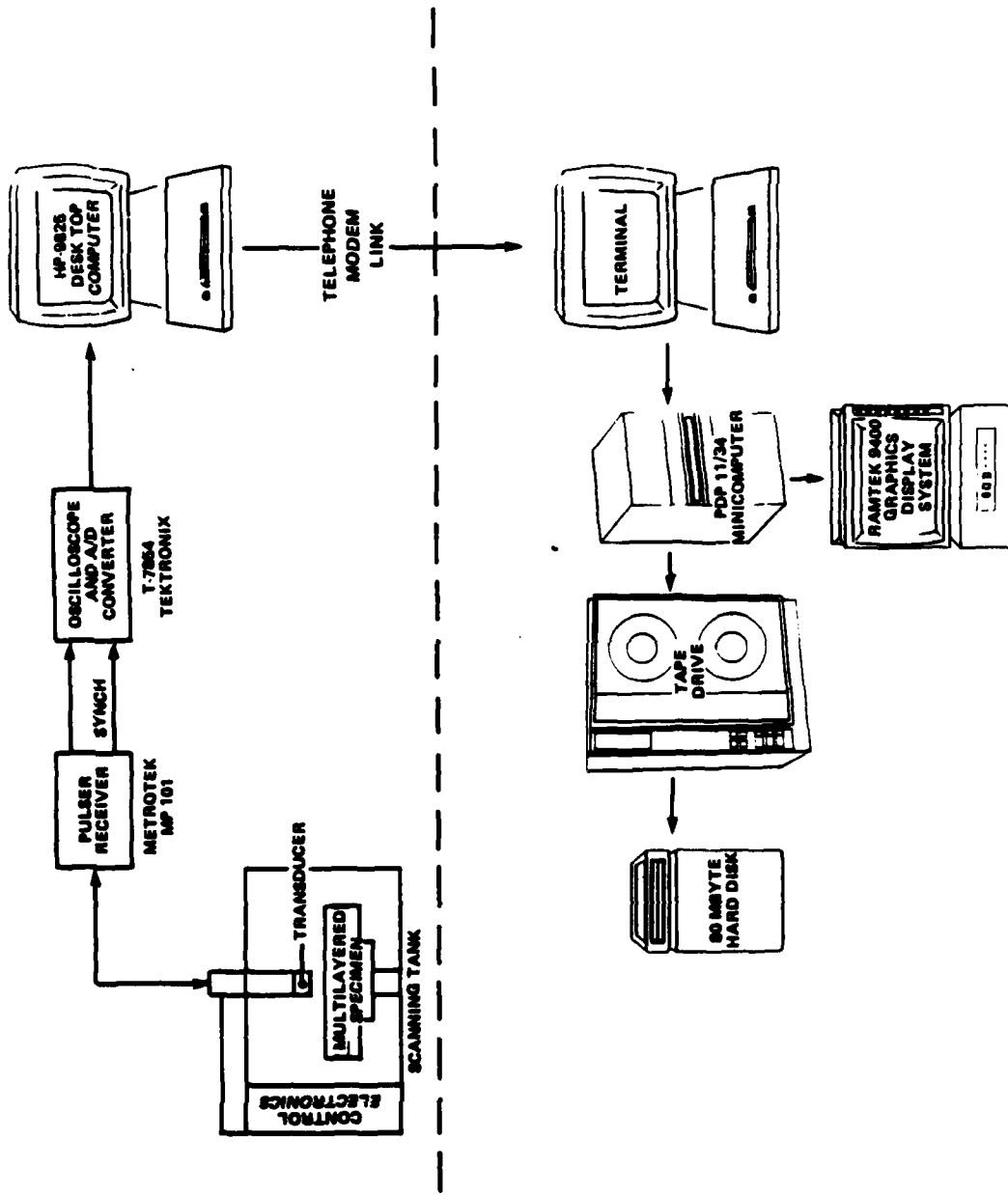


Figure 4.3 ULTRASONIC DIGITAL DATA PROCESSING CONFIGURATION

NAVAL SURFACE WEAPONS CENTER, WHITE OAK, MARYLAND
MATERIALS EVALUATION LABORATORY

	DATE	23 December 81
	TIME	10:00 A.M.
SAMPLE SPECIFICATIONS		
SNP	SAMPLE DESCRIPTION	0.25 in. bronze, 0.125 in rubber Epoxy layer in between .032 in Bronze on top
SNP	SAMPLE ID NUMBER	#3 (.032 in epoxy) /
SNP	WAVEFORM IDENTIFICATION #	BRU3.NEZ
SCANNER TESTING DESCRIPTION		
SCN	SCANNER MAKE AND SERIAL NUMBER	U.S. Automation 450 Series PA04349
SCN	TYPE OF ULTRASONIC TESTING	IMMERSION
SCN	TEST MODE(PULSE/ECHO,PITCH/CATCH)	PULSE-ECHO
SCN	WAVE PROPAGATION MODE	LONGITUDINAL
SCN	BEAM ENTRY ANGLE	NORMAL INCIDENCE
SCN	WATER TEMPERATURE	72°F
SCN	TX TO FRONT SURFACE DISTANCE	120 mm
SCN	RX TO BACK SURFACE DISTANCE	N/A
TRANSDUCER SPECIFICATIONS		
TX/RX	TRANSMITTER MODEL AND SN	KB AEROTECH, GAMMA-SERIES,0.25 in.
TX/RX	RECEIVER MODEL AND SERIAL NO.	#2308
TX/RX	NOMINAL CENTER FREQUENCY	5.0 MHZ
PULSER/RECEIVER SPECIFICATIONS		
P/R	PULSER MODEL AND SERIAL NUMBER	METROTEK MP203 M23068
P/R	RECEIVER MODEL AND SERIAL NUMBER	METROTEK MP101 M110881
P/R	PULSE AMPLITUDE SETTING	11 0'CLOCK
P/R	REP RATE	1.0 kHz
P/R	DAMPING	5 0'CLOCK(MAXIMUM)
P/R	FILTER	4.0 MHZ
P/R	ATTENUATION	0 dB
ANALOG TO DIGITAL CONVERTER SPECIFICATIONS		
A/D	CONVERTER MODEL AND SERIAL NUMBER	T7854,TEKTRONIX B03108
A/D	COUPLING	AC
A/D	INPUT OFFSET	0 v
A/D	TIME DELAY	98.4 MICROSECS
A/D	TIME/DIV SETTING	2 MICROSECS
A/D	VOLTS/DIV SETTING	0.02 v/div
A/D	NUMBER OF AVERAGE TRACES IN WAVEFORM	100
A/D	TRIGGER ORIGINATING FROM	P/R SYNC
A/D	TRIGGER SOURCE	EXTERNAL
A/D	TRIGGER SLOPE	POSITIVE
A/D	TRIGGER COUPLING	DC
A/D	TRIGGER LEVEL	12 0'CLOCK

COMMENTS: Positioned over area with no epoxy. Presumably air or water in between rubber and bronze.

Figure 4.4 HEADER SHEET

Although most of the specimens were examined in immersion mode, a few waveforms were also recorded in contact mode for material property determination. In both cases the same transducer(s) were used: they were either a single (or pair of) 5.0 MHz or 2.25 MHz transducer.

ULTRASONIC SIGNAL PROCESSING

INTRODUCTION

Signal processing involves computer enhancement of ultrasonic data that are bandlimited and the available information in the signal is not apparent to the naked eye. The primary reason for utilizing enhancement schemes is for improving signal detectability using manual or automatic means. In addition signal processing procedures allow for suppressing unwanted frequencies while enhancing others which may be required for separating signal from noise, for suppressing unwanted reverberations and for performing frequency dependent compensation when higher frequencies have been more attenuated than the lower.

The chapter discusses various signal processing methods used on recorded digital data from bronze-rubber specimens. The methods include: standard, linear filtering using fast fourier transform techniques which allow low- high- and band-pass filtering in the frequency domain and the use of finite impulse response filters (FIR); deconvolution methods for bandwidth enhancement and for normalizing signals [3], and cepstral processing methods to minimize unwanted reverberations and/or to separate overlapped signals [9]. These methods were evaluated on signals simulated by the model and on digital data collected at the laboratory.

FILTERING

Both time domain and frequency domain filtering methods were employed on these data to minimize the effects of broadband noise. A Finite Impulse Response (FIR) filter was designed in the time domain. Advantages of such a filter are: easy computer implementation and non-recursiveness of filter output, extremely sensitive band-pass and band-reject characteristics which can be selected at the user's discretion, linear phase filter impulse response resulting in very little distortion in the filtered output, and the ability to "downsample" i.e., effect sampling at lower rates, more effectively than with conventional filters.

Filtering with an FIR is the result of convolving an input series x_j with a filter coefficient series a_j to produce:

$$y_n = \sum_{j=1}^K a_j x_{n-j}$$

The coefficients a_j (also called "taps") are selected so as to produce the effect desired: if band-pass filtering is necessary then the number and type of coefficients are automatically selected to produce the given effect.

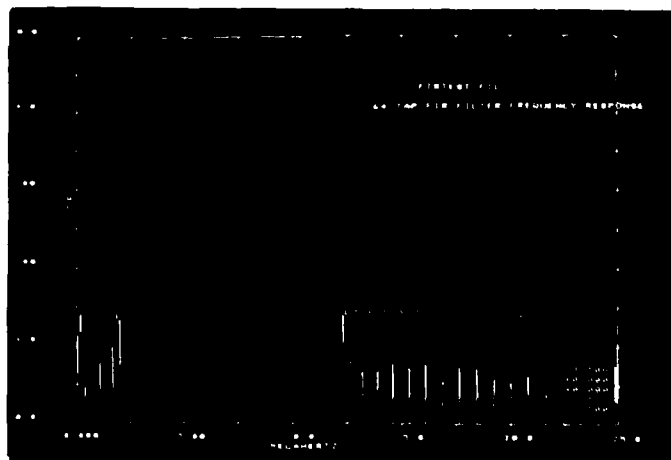
The impulse and frequency response of a 64-tap bandpass filter, designed to pass all frequencies between 8% and 20% of the sampling frequency is shown in Figure 5.1. The top picture is the impulse response and the bottom shows the frequency response. It can be seen that in the pass band the ripple is almost negligible, while the response in the rejected regions is 60 dB below the response in the pass band.

The filter was applied on data collected from a bronze-rubber specimen. Figure 5.2 shows the pulse echo response from such a specimen. The bronze and rubber thicknesses were nominally 6.35 and 3.175 mm, respectively. The center frequency of the transducer used was 5.0 MHz and its frequency response is shown in Figure 3.7. The sampling rate was 50.0 MHz. The presence of high frequency noise can be seen in the entire trace, and is revealed in the spectral plot shown at the bottom of Figure 5.2. The filtered trace using the FIR band pass filter is shown in Figure 5.3. It can be seen that the phase relationship of the signals is well preserved (compare to raw data in Figure 5.2), with a reduction in the high frequency noise.

The performance of the FIR filter was compared with a conventional FFT filter wherein bandpass filtering was achieved in the frequency domain, via FFTs. For FFT filtering, the input signal is transformed into the frequency domain via an FFT algorithm. The signal is then bandpassed filtered and windowed using a Hanning window. The resulting output is then inverse transformed back into the time domain. The FFT filtered trace is shown in Figure 5-4. It can be seen that while high frequency noise has been reduced the number of cycles in each signal is more in the filtered trace. This is because of ringing introduced by FFT filtering, which is reduced somewhat by the Hanning window, but not fully suppressed. Each return has more cycles in the filtered trace than in the original. The effect of additional cycles in the signal is that the phase relationships are altered, and thus any change in phase because of a flaw (or gap instead of an epoxy layer, for example) may not be faithfully preserved.



IMPULSE RESPONSE

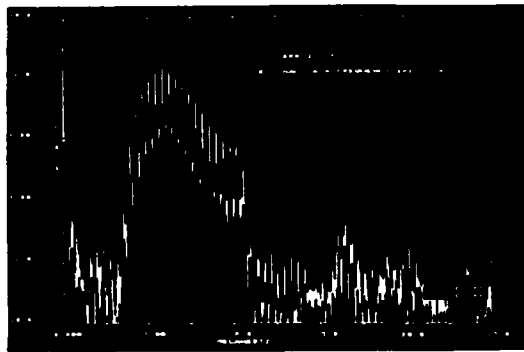


FREQUENCY RESPONSE

Figure 5.1 FIR BANDPASS FILTER

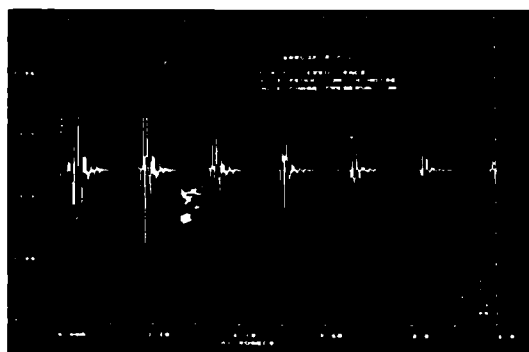


TIME SERIES

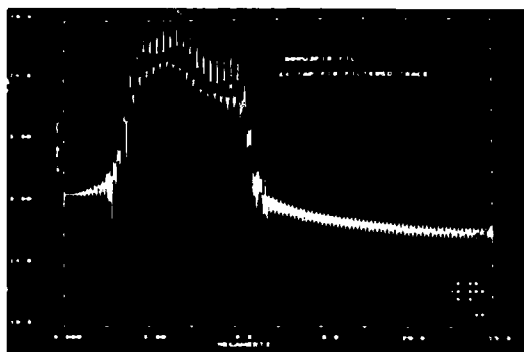


FREQUENCY RESPONSE

Figure 5.2 ORIGINAL TRACE

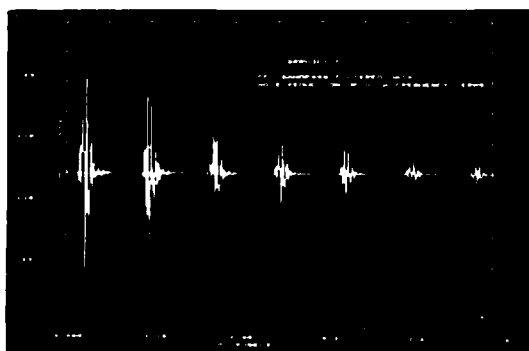


TIME SERIES



FREQUENCY RESPONSE

Figure 5.3 FIR FILTERED



TIME SERIES



FREQUENCY RESPONSE

Figure 5.4 CONVENTIONAL FILTERING

To compensate for frequency-dependent attenuation due to rubber, a preemphasis filter was designed. The presence of frequency-dependent attenuation was illustrated in Figure 3.12. It was argued that the attenuation model was log linear, i.e., the difference in log spectra, for equal distances, was dependent linearly in frequency. The negative slope was inversely proportional to a parameter defined as the Q , which was material dependent. High Q materials are less attenuative than low Q materials.

A flow chart for implementing such a filter is shown in Figure 5.5. The input signal is transformed via an FFT and then multiplied by $\exp(\alpha f)$ where α is dependent on the material Q and filter frequency. The operation is carried out over a limited bandwidth, preferably over the bandwidth over which the Q measurement was made. The inverse FFT will be the compensated signal.

An example of this application is shown in Figure 5.6. The trace shows the front and back surface signals from rubber immersed in water; the transducer was rated at 5.0 MHz and the sampling rate was 100 MHz. The front and back signals are shown in separate plots in Figure 5.7. The front and back surface signals should be π radians out of phase alignment because the front surface reflection occurs at the water-rubber interface and the back surface at the rubber-water. While the first motion in the front surface signals is easily discernible as negative-going, the corresponding positive-going first motion is not clear in the back surface signal. Also there are more cycles evident in the front surface return than in the back surface return. If there were no frequency dependent attenuation, the signals should be exact replicas of each other, except for a π radian phase shift. To compensate for the attenuation loss suffered in rubber the back surface signal was frequency-compensated to produce the signal at the bottom in Figure 5.7. It can be seen that the compensated signal and the front surface are opposite in phase and are more similar -- as they should be if there were no frequency dependent attenuation. The advantage of frequency compensating filtering is that phase relationships can be very accurately preserved and hence change at the interface (i.e., flaws) can be easily monitored.

DECONVOLUTION

Deconvolution has been used traditionally to computer enhance bandwidth for additional resolution. This will enable one to separate two overlapped signals such as those received from the front and back surface of epoxy. If the epoxy thickness is 0.5 mm, for example, then the round trip transit time for an ultrasonic pulse is 0.36 μ s (velocity:

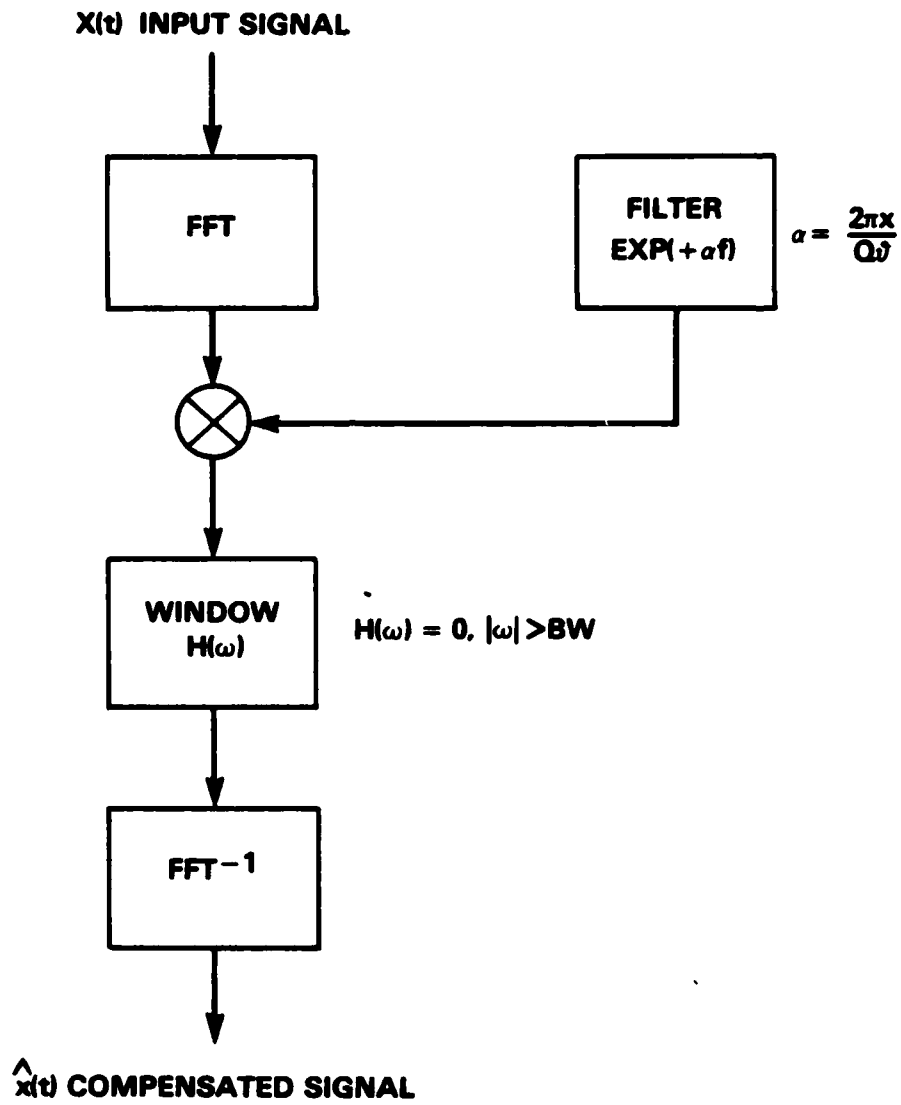


Figure 5.5 FREQUENCY COMPENSATING FILTER

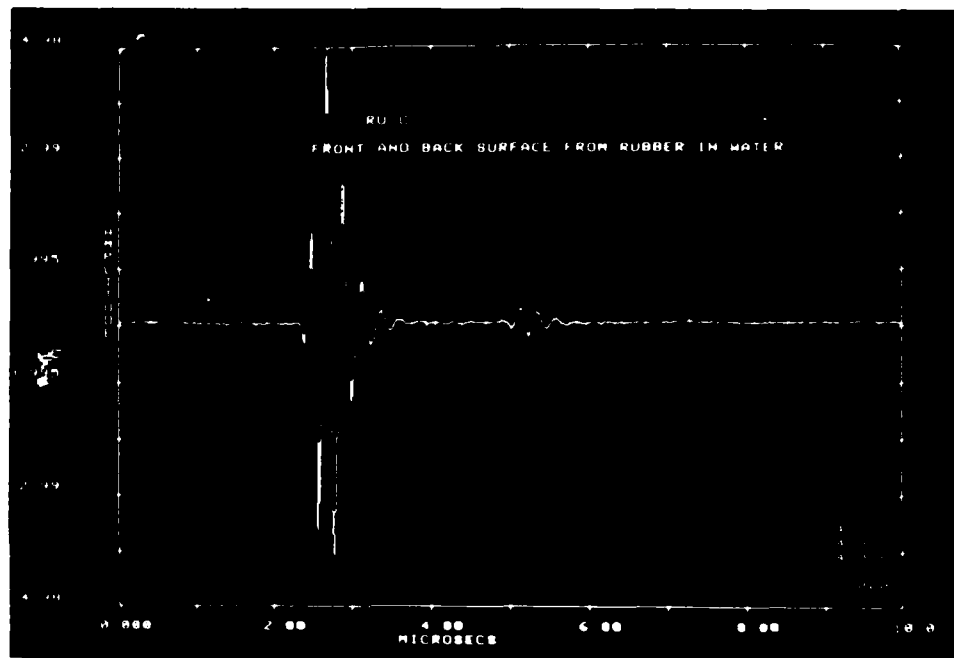
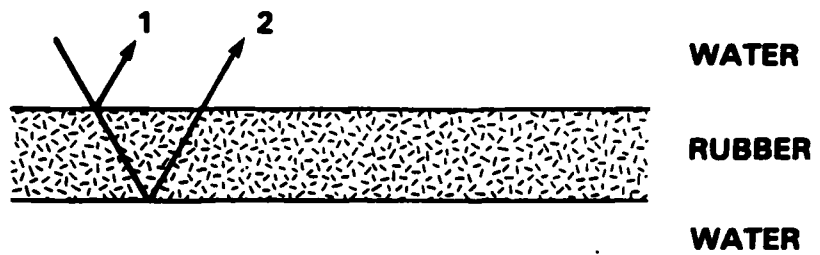
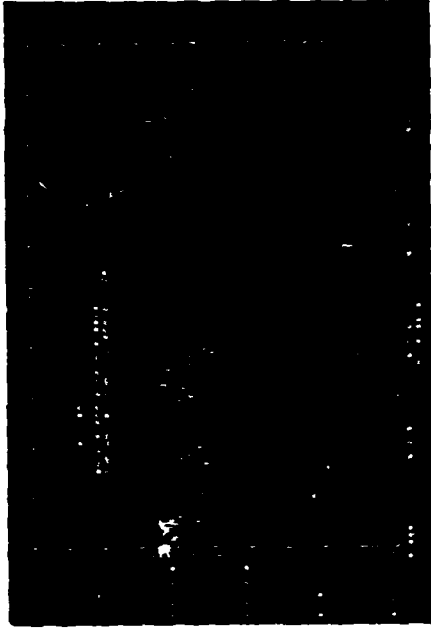


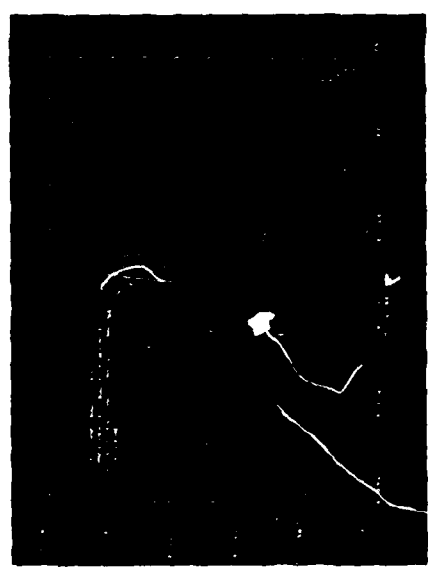
Figure 5.6 FRONT AND BACK SURFACE RESPONSE



BACK SURFACE



FRONT SURFACE



COMPENSATED BACK SURFACE

Figure 5.7 FREQUENCY-COMPENSATING FILTER

2.75 mm/ μ s). In other words, the pulse 3 dB bandwidth should exceed 2.75 MHz ($1/0.36$ MHz) to visually separate the two interfaces. In addition, the pulse duration should be less than 0.36 μ s, which was often not attainable; it was typically 0.80 μ s.

Deconvolution can be implemented in time domain as well as in the frequency domain, although the latter implementation is more widespread. Two signals are required. The first is the signal to be deconvolved and the second a reference signal whose characteristics should include everything that is to be removed in the first. Usually the reference signal is a backwall echo which is characteristic of the transducer frequency resonance. The flow chart for implementing the algorithm is shown in Figure 5-8. The signal FFTs are divided in the frequency domain. Although the operation appears innocuous, the dividend is not well defined for small values of the divisor, especially at frequencies where the reference has very little energy (i.e. at the poles). At the poles, the resulting inverse transform "blows up" and causes unstable oscillation in the time signal. Thus a "fudge factor" related to the signal-to-noise ratio is added to the divisor to ensure a finite value at the singular points. The resulting signal should have broader bandwidth and hence greater resolution.

Deconvolution was attempted on the bronze-rubber specimen with a layer of epoxy in between. A flow chart is shown in Figure 5.9 for deconvolving the bronze-rubber signal. Before and after deconvolution the signals were prefiltered to retain only the signal bandwidth.

Figure 5-10. shows the results before and after deconvolving. It is evident that in the original trace the signal consist of reverberation within bronze while the returns from the lower layers are completely submerged in the tail end of the bronze reverberations. (Labeled 1, 2, etc.). After deconvolution the echoes labelled A, B, etc. are more evident as a result of the enhanced resolution. The smaller amplitude of the signal testifies to the fact that significant portion of the energy is trapped within the bronze layer.

While enhancing resolution is desirable, deconvolution can be further used in eliminating the bronze reverberations as much as physically possible. The scheme for this procedure is shown in Figure 5.11. The signal consists of the reflection series due to bronze (I_{BR}) plus everything else (called I_{REST}); both are convolved with a transducer signal. The reference in this case consists of the bronze reverberations which is obtained by collecting the data from a bronze block of identical dimensions. The resulting deconvolved spectrum will consist of two terms: one which is all pass (which is 1), the other is approximately the ratio of spectrum of I_{REST}

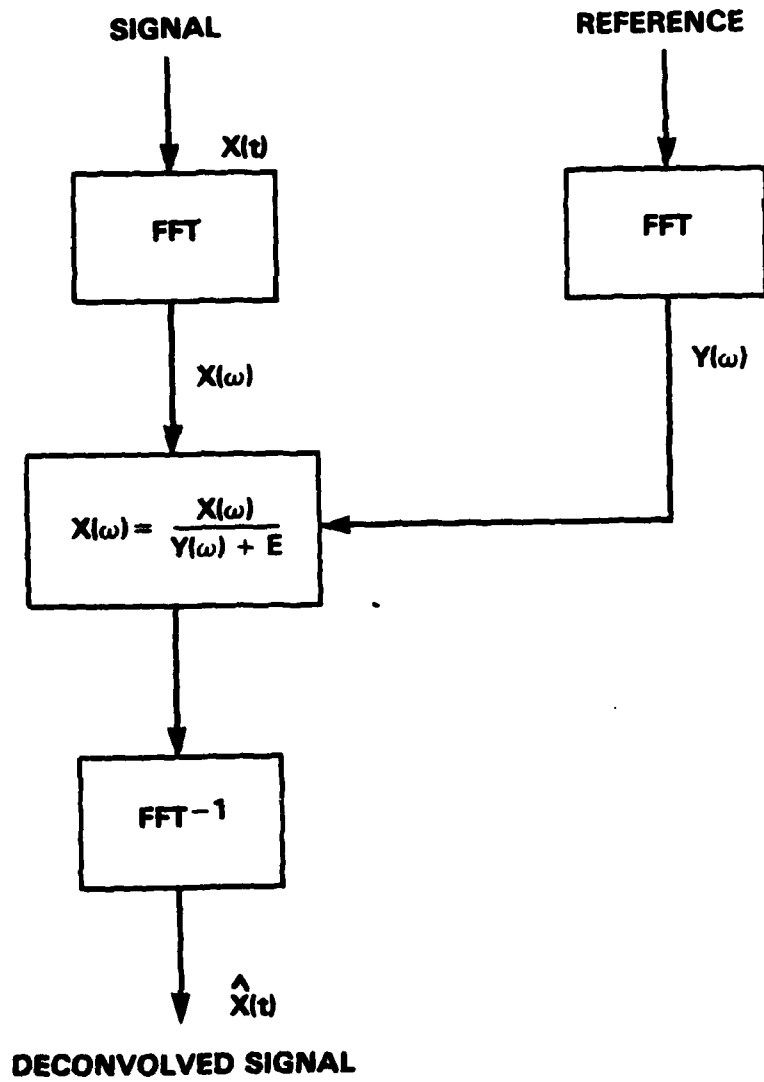


Figure 5.8 STEPS IN DECONVOLUTION

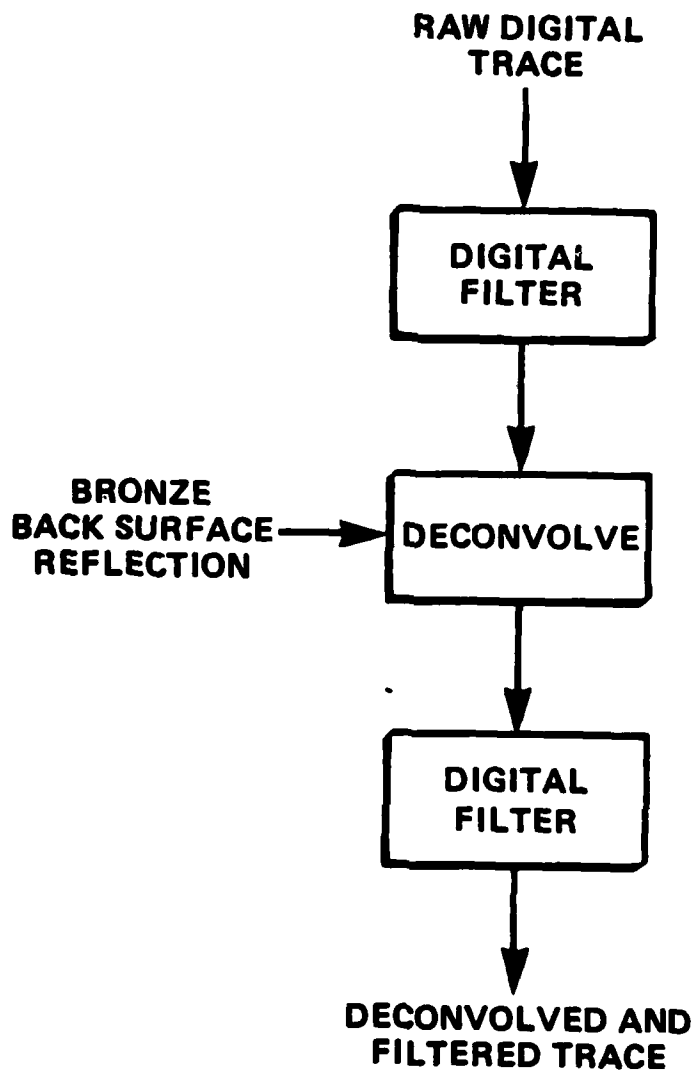
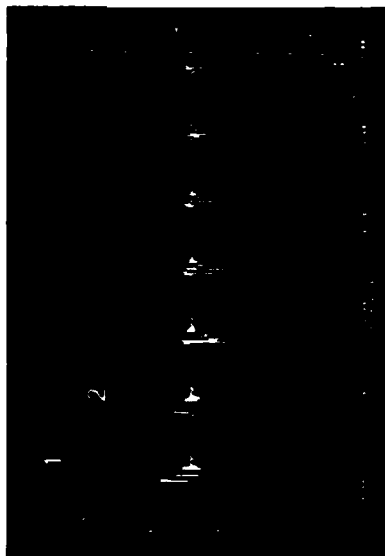
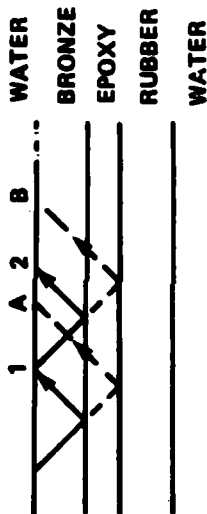
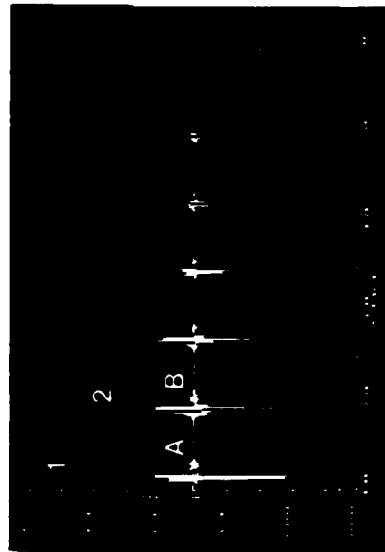


Figure 5.9 DECONVOLUTION FOR INCREASED RESOLUTION



RAW DIGITAL TRACE



DECONVOLVED AND FILTERED

Figure 5.10 INCREASED RESOLUTION IN BRONZE-RUBBER INSPECTION BY DECONVOLUTION

**REFERENCE
BRONZE
SPECIMEN**

**"GOOD"
BRONZE-RUBBER
SPECIMEN**

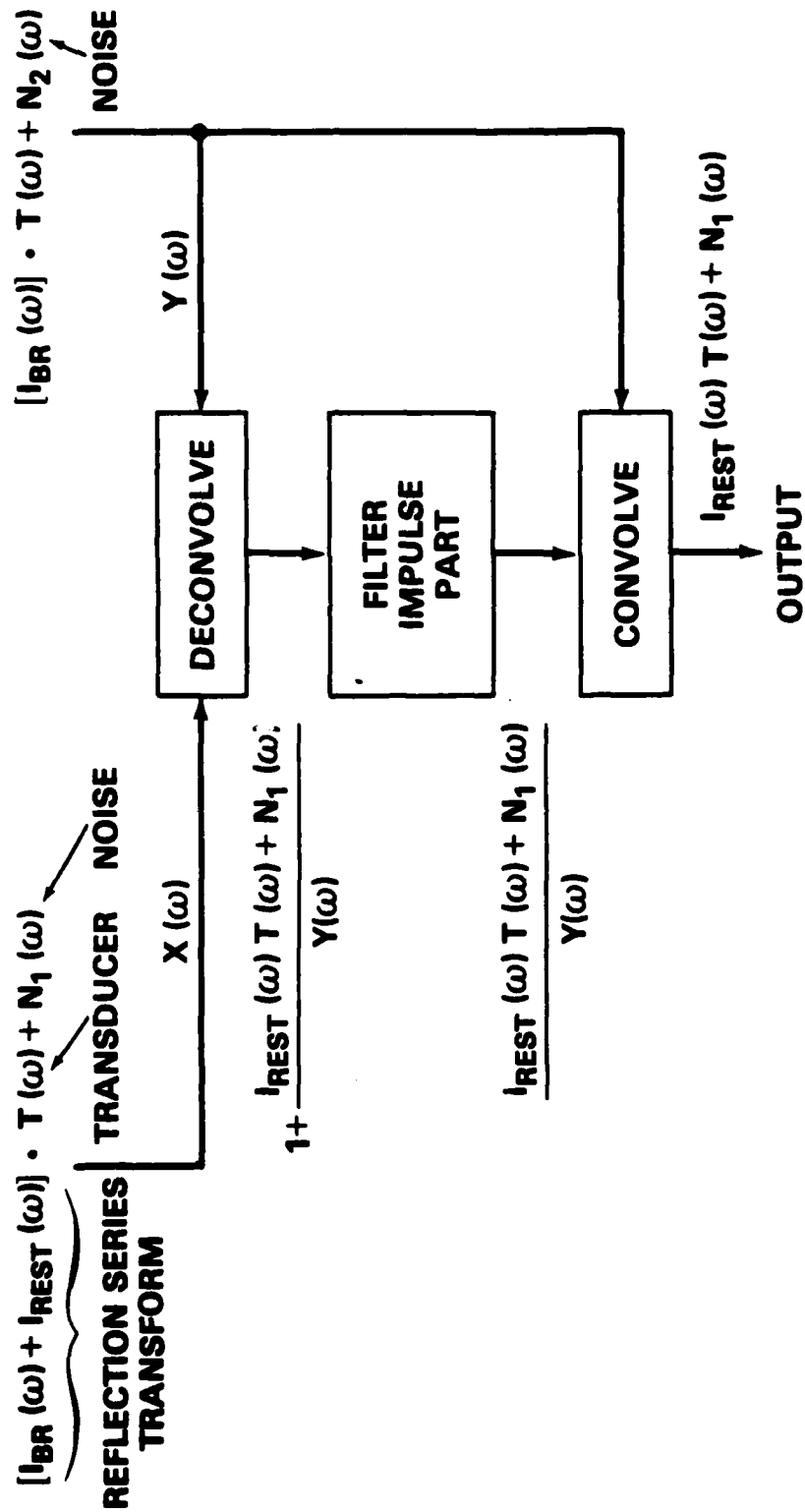


Figure 6.11 DECONVOLUTION OF BRONZE REVERBERATIONS

and I_{BR}. By filtering the all pass contribution (which is an impulse at the origin), and multiplying the resultant with the reference series, the series due to the bronze will have been eliminated, theoretically.

The results of such a dereverberation process are shown in Figure 5.12. The original and deconvolved are shown in the top. The dereverberated signal wherein the bronze reverberations have been eliminated is shown at the bottom. Elimination of the bronze series is validated by two observations:

- o the amplitude scales on the bottom plot are an order of magnitude less than that in the deconvolved series.
- o the rate of decay of pulses in the dereverberated series do not fit the pattern of decay observed for the original bronze series.

In summary, therefore, deconvolution and dereverberation greatly enhance the S/N ratio and minimize unwanted dominant reverberations.

Another point to note is the similarity of the dereverberated series and the simulated ideal reflection series from the same specimen shown in Figure 3.5. The two major series in that figure consist of the negative impulses due to bronze and the positive impulses which have undergone an additional transit through the epoxy layer. Eliminating the bronze reflections series will result in, primarily, the positive impulse series.

CEPSTRAL PROCESSING

The cepstrum - a relatively new method -- has been demonstrated on sonar, radar and image processing applications for separating two or more overlapped responses. The basis for the cepstrum lies in the fact that when two signal echoes are combined then the composite signal can be modeled as a convolution of primary signal with a pair of impulses : one at the origin and another at a time delay corresponding to echo arrival time. The complex FFT of this composite signal will be the multiplication of the primary signal FFT and FFT of the impulse sequence; the latter impulse produces a cosinusoidal ripple in addition. The logarithm of the FFT is taken to separate these multiplied components. The components are now additive. This transformation is the cepstrum and standard linear filter procedures can be used to remove any one of the two components.

Its relevance to multilayered NDE lies in the fact that returns from the bronze-epoxy and epoxy-rubber interface will

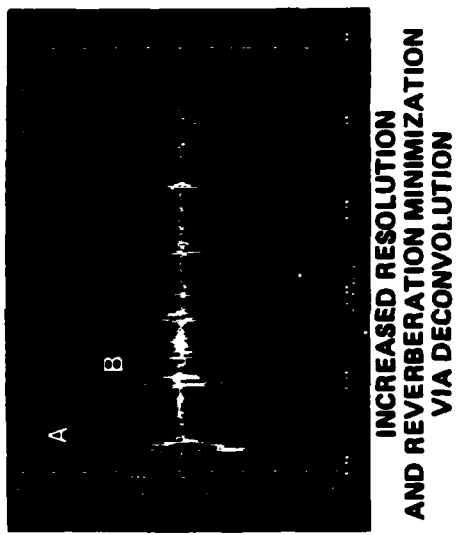
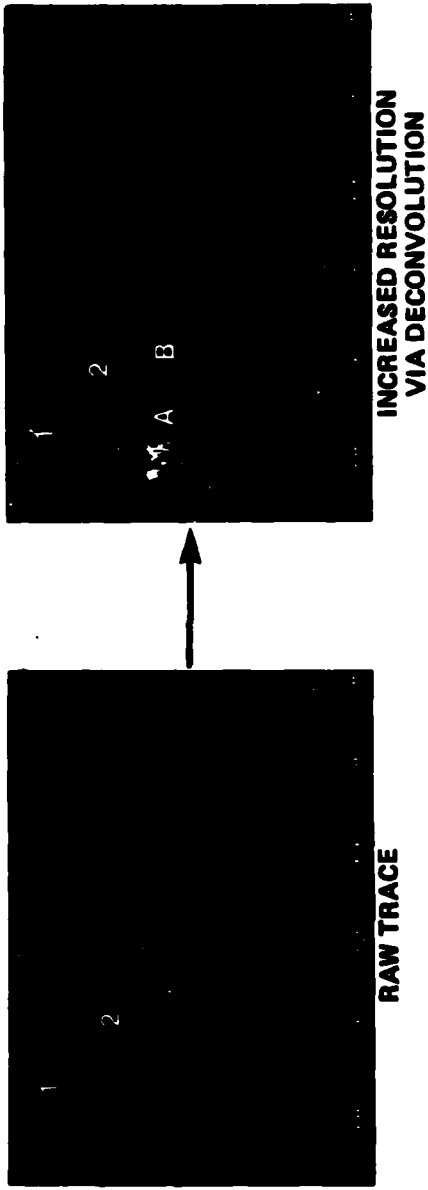


Figure 5.12 MINIMIZATION OF BRONZE REVERBERATIONS

overlap because of finite bandwidth, making visual separation difficult. If there were a flaw, such as delamination at the second interface, then a change in that signal characteristic will not be easily discerned. By being able to separate out the two responses one can carefully monitor the amplitude and spectral characteristics to determine presence of misbond in the lower layer.

The steps in extracting the two components are illustrated in Figure 5.13. The scheme is called the complex cepstrum, because it retains amplitude and phase information to extract the time signals. The signal plus echo is transformed into the frequency domain via the FFT and the complex logarithmic taken. The real part is the log magnitude and the imaginary part is the phase angle. Because the phase is module 2π , there will be discontinuities at variations from $-\pi$ to π and vice versa. The phase is made continuous by an "unwrapping" procedure which adds a 2π factor to the phase angle each time such a change is made. After this operation a linear phase trend is introduced, which is removed because it will introduce a large amplitude delay term in the time domain. The inverse FFT is taken to produce the complex cepstrum, which will consist of the cepstrum of the primary wavelet and an impulse at a location corresponding to the time delay. After removing the impulse by linear filtering method, and retracing the steps, the original primary wavelet can be recovered, i.e., the bronze-epoxy return for multi-layered NDE. The difference between the composite and the recovered primary will be the echo signal, i.e. the return from epoxy-rubber.

Application of cepstral filtering to the bronze-epoxy-rubber interface signal is detailed below. The original data trace is in Figure 5.2.

The steps for complex cepstrum processing are shown in Figure 5.14. The original data trace is filtered using an FIR filter and then processed by the cepstrum. For the cepstrum, only a finite window centered around the return of interest from the trace is used. The primary signal is first recovered by cepstral filtering. This will be the first interface signal (i.e., bronze-epoxy). The recovered primary is then subtracted from the original to produce the recovered second interface signal (i.e., epoxy-rubber). To further validate the degree of similarity between the primary and echo, the correlation coefficient can be computed from the cross-correlation between the two signals. Both the magnitude of the coefficient and its delay can be used to validate results.

Figure 5-15 shows the results after processing the first major signal observed in Figure 5.2. The FIR filtered data are shown on top of Figure 5.15. The high frequency noise

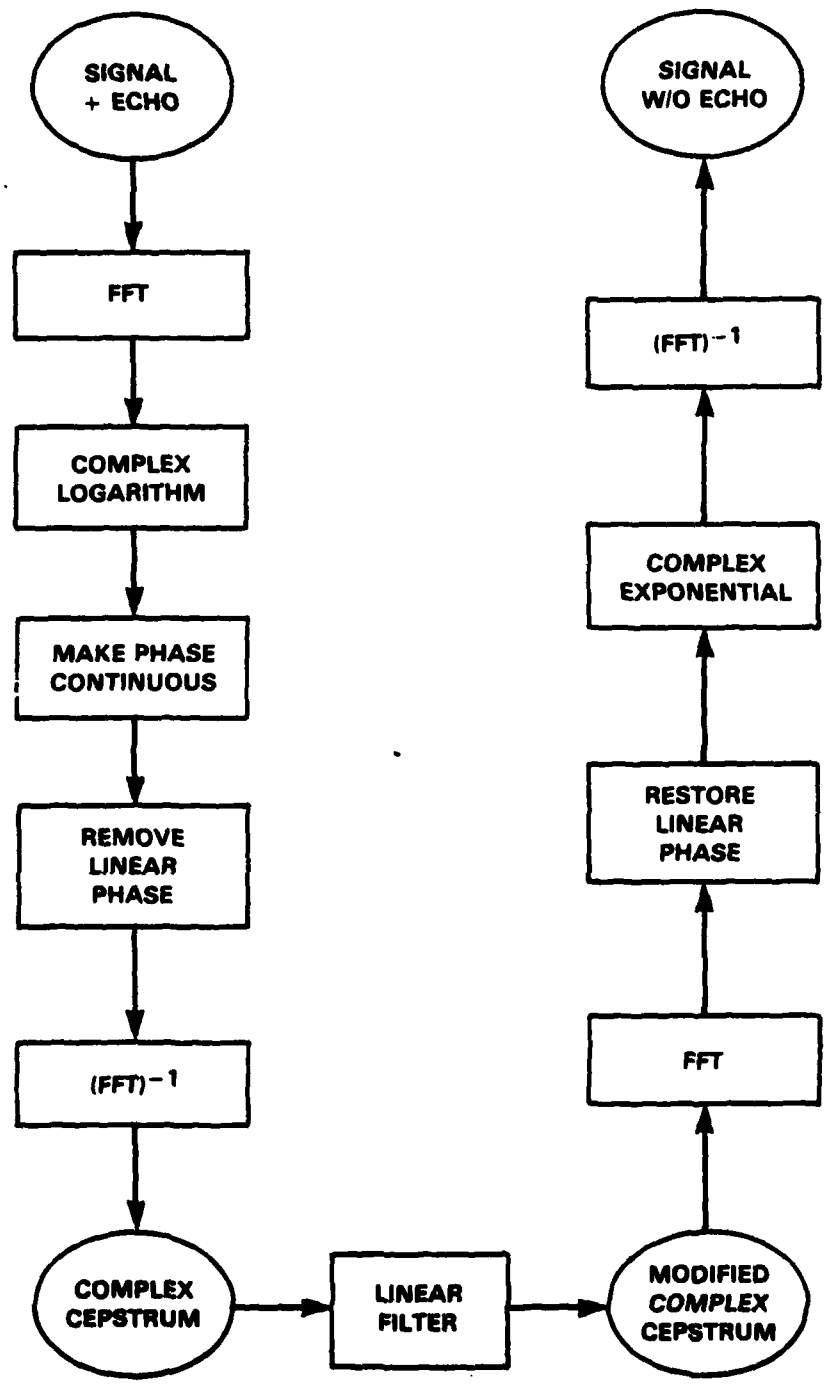


Figure 5.13 STEPS IN COMPLEX CEPSTRUM COMPUTATION

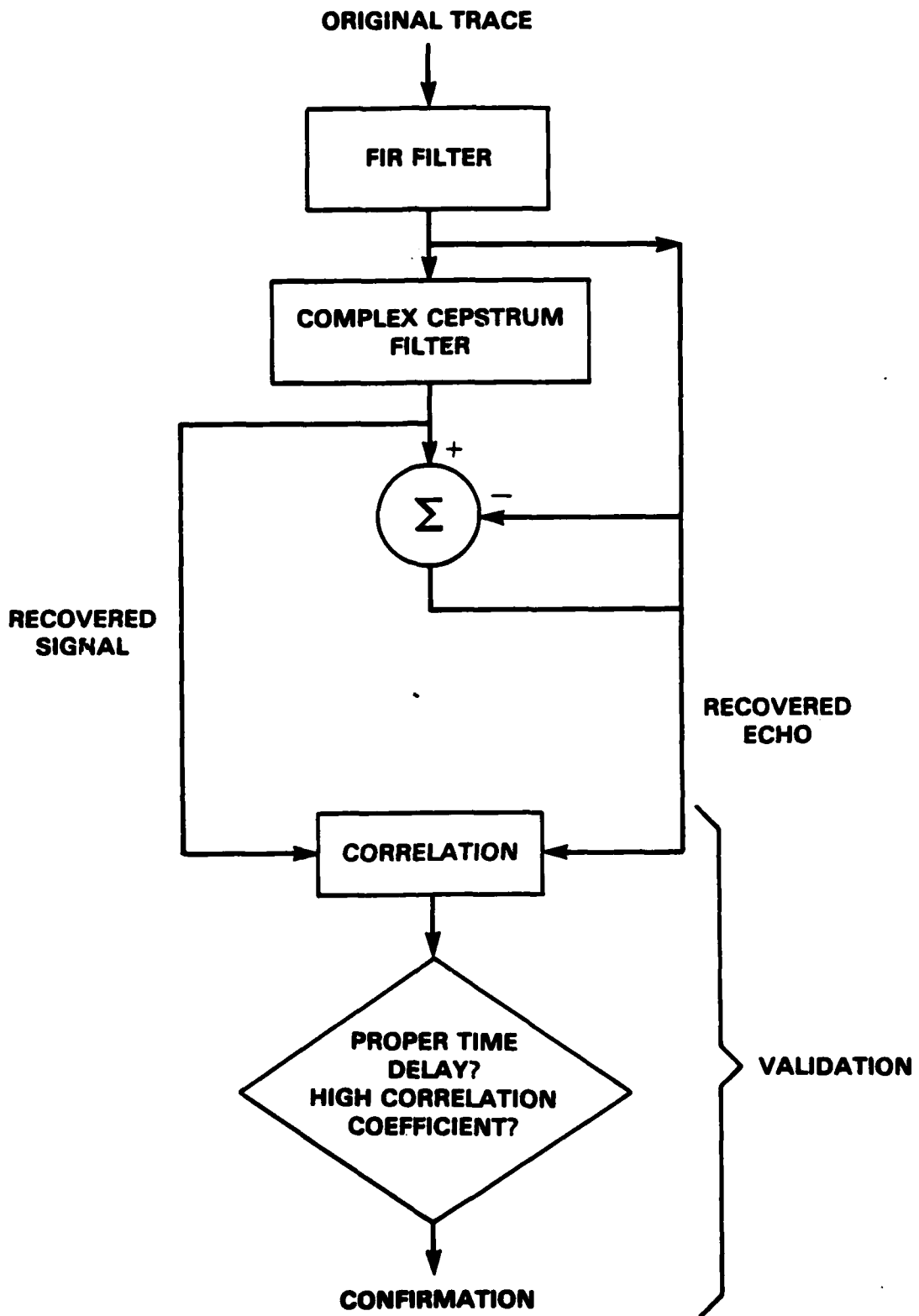
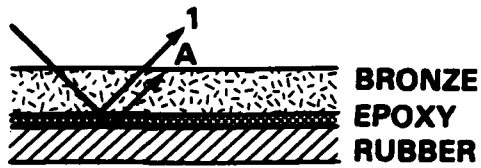
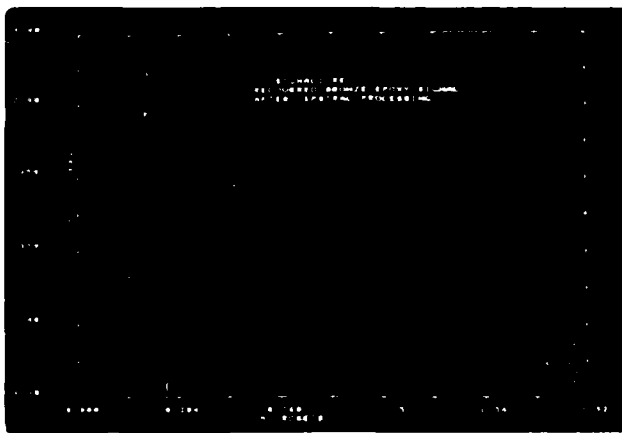


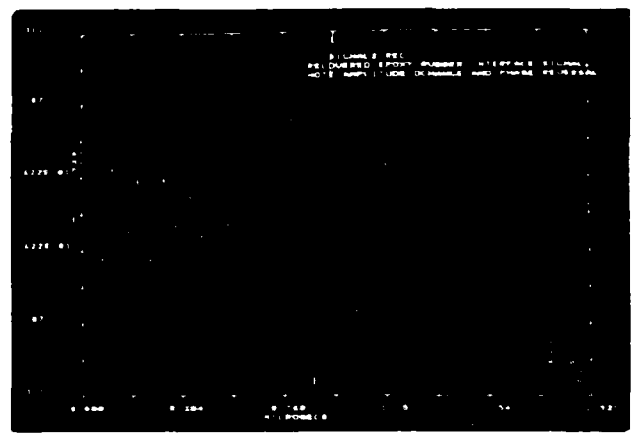
Figure 5.14 COMPLEX CEPSTRUM FILTERING



FIR FILTERED



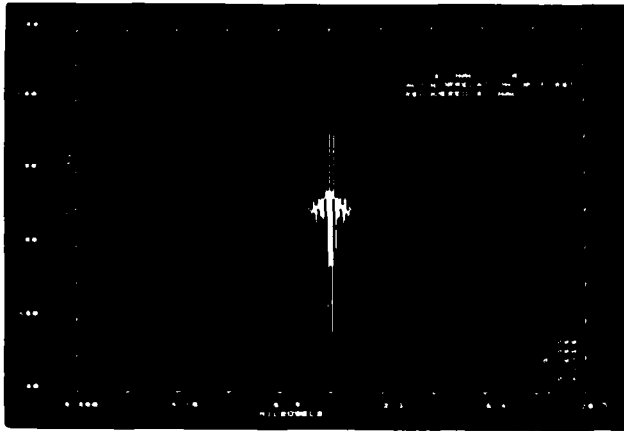
**RECOVERED SIGNAL
(BRONZE-EPOXY)**



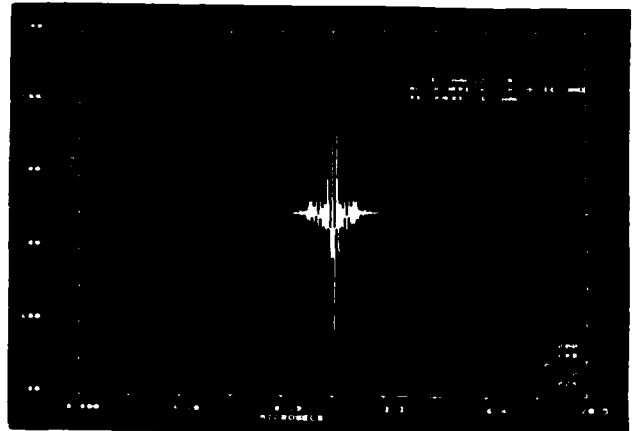
**RECOVERED ECHO
(EPOXY-RUBBER)**

**RATIO OF MEASURED AMPLITUDES: 14.13
RATIO OF REFLECTION COEFFICIENTS: 12.55**

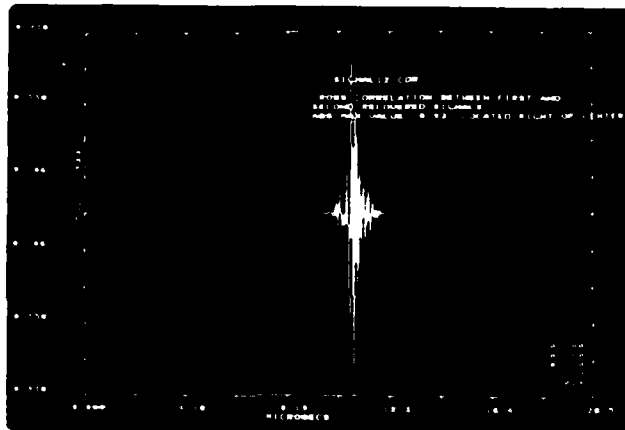
Figure 5.15 CEPSTRUM PROCESSING



**AUTOCORRELATION
OF SIGNAL RECOVERED**



**AUTOCORRELATION
OF ECHO**



**CROSS CORRELATION
OF SIGNAL AND ECHO**

**MAXIMUM CORRELATION 93%
DELAY TIME 0.60 μ s \Rightarrow 0.72mm**

Figure 5.16 CORRELATION OF RECOVERED SIGNAL AND ECHO

SUMMARY OF RESULTS AND RECOMMENDATIONS

A computer based acoustic model has been developed for the NDE of multilayered structures. The model is applicable for normal or off-normal incident excitation, with receiver in pulse-echo, pitch-catch or in array mode. The model can simulate the observed signal for arbitrary frequency response of the transmitting and receiving transducer. In addition the model considers attenuative and mode conversion effects in each layer in predicting the ultrasonic response.

Ultrasonic digital data were processed from a bronze-epoxy-rubber multilayered structure to validate model and to determine suitable digital signal processing methods. These methods included: compensating filters which were frequency dependent to offset attenuation in the media; deconvolution for bandwidth enhancement and to improve resolution, and the cepstrum -- a relatively new method -- to separate the overlapped response from different interfaces.

Computer model simulation was used successfully to predict the response from this structure. In particular, the model output dictated the inspection configuration and signal processing methods to be used on the data.

Based on these results, it is recommended that angled beams be used to inspect the structures instead of the traditional normal incidence, pulse-echo methods used. It is further recommended that validation of the angled beam model be carried out by analyzing and processing digital data from these structures.

REFERENCES

- [1] Liber, T., et.al. in Nondestructive Evaluation and Flaw Criticality for Composite Materials, ASTM STP 696, American Society for Testing and Materials, 1978, pp 5-25.
- [2] Hironaka, M.C., et.al. "Detection of Voids Underground and Under Pavements." Technical Note N-1449, Civil Engineering Lab., Naval Construction Battalion Center, Port Hueneme, CA.; August 1976.
- [3] Robinson, E.A. and S. Treitel. Geophysical Signal Analysis. Prentice-Hall. Englewood Cliffs, N.J.; 1980.
- [4] Ewing, W.M., Jardetsky, W.S., and F. Press. Elastic Wave in Layered Media. McGraw-Hill. 1957.
- [5] Scott, W.R., "Ultrasonic Reflection Spectrum Analysis for NDE of Periodic Layered Media." JASA, Vol. No. 61, No. 6, June 1977.
- [6] Knopoff, L., "Q," Reviews of Geophysics, 2, #4, Nov. 1964.
- [7] Kak, A.V. and K.A. Dines, "Signal Processing of Broad-band Pulsed Ultrasound." IEEE Trans on Bio. Eng. July 1978.
- [8] Futterman, "Dispersive Body Waves," J. Geo. Research 67, pp. 5279-5291, 1962.
- [9] Shankar, R. and R.N. McDonough, "Ultrasonic Measurement of Defects in Materials using Cepstral Processing." Proc. of IEEE Conf. on ASSP, April 1978.

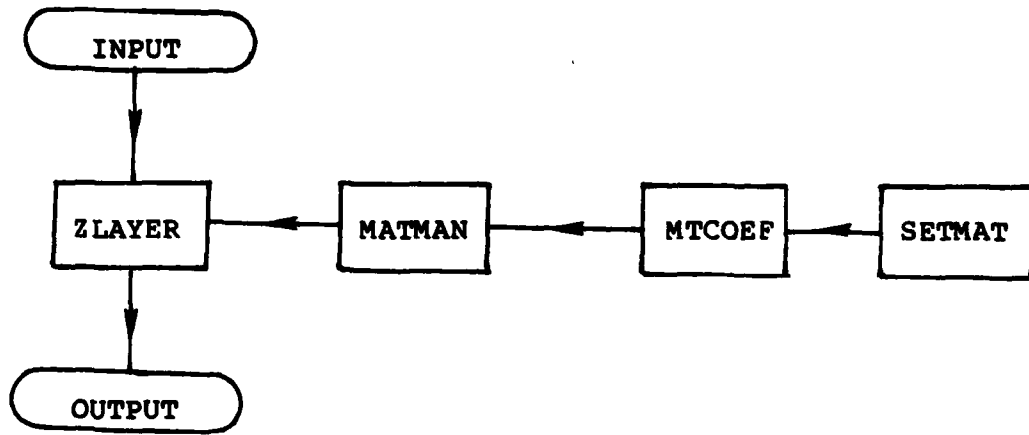
APPENDIX
FLOW CHART OF ACOUSTIC NDE COMPUTER MODEL

MULTILAYERED MODEL

INTRODUCTION

The Multilayered Model describes waveform response for an arbitrary multilayered structure. Flexible enough to handle different scenarios such as pulse echo or through transmission response, the model ultimately generates a time series and stores the data in a disk file. Each individual run of the computer model requires program-user input of file names and model options. The time series data may be displayed using a graphics display or similar device. A brief description of the program modules and necessary files comprising the multilayered model follows.

FLOWCHART OF THE MULTILAYERED MODEL



PROGRAM MODULES

ZLAYER generates a waveform response for a given multilayered structure. Using a beam angle or normal incident wave, and studying the pulse echo or through transmission response, ZLAYER creates a file that contains the real, imaginary and absolute value parts of the waveform. The program user has the option to either generate a new set of transmission and reflection coefficients for the multilayered structure, or to process a pre-created file. Recursive polynomials describing the waveform response are computed with the appropriate coefficients.

MTCOEF computes the matrix M whose elements reflect some of the acoustical properties of 2 adjacent layers. M has the form

$$\begin{bmatrix} -1 & 0 & M_{13} & M_{14} \\ 0 & 1 & M_{23} & M_{24} \\ 1 & 0 & M_{33} & M_{34} \\ 0 & -1 & M_{43} & M_{44} \end{bmatrix}$$

where $M_{13}, \dots, M_{43}, M_{14}, \dots, M_{44}$ are layer-dependent features. The matrix M is used to generate the reflection and transmission coefficients of incident waves through the matrix equation

$$M * \begin{bmatrix} R_{pp} \\ R_{ps} \\ T_{pp} \\ T_{ps} \end{bmatrix} = \begin{bmatrix} 1 \\ 0 \\ 1 \\ 0 \end{bmatrix} \quad \text{in the case where P waves are incident.}$$

When shear waves are incident, a slight change is made in the matrix equation to

$$M * \begin{bmatrix} R_{sp} \\ R_{ss} \\ T_{sp} \\ T_{ss} \end{bmatrix} = \begin{bmatrix} 0 \\ 1 \\ 0 \\ 1 \end{bmatrix}$$

MATMAN takes an arbitrary multilayered structure and computes the reflection and transmission coefficients of an incident wave. Processing sequentially through adjacent layers, MATMAN computes a set of reflection and transmission coefficients for both the downgoing and upgoing waves at each interface. Based on the wave of interest in each layer, the appropriate reflection and transmission coefficients are selected for the waves in both directions, and are stored in a file that is used in the module ZLAYER.

SETMAT retrieves the real and imaginary parts of the elements in the complex matrix computed in the module MTCOEF, and stores the numbers in 2 separate matrices. Upon re-entry into the program module MATMAN, the 2 real matrices are used to compute the inverse of the original complex matrix.

FILES

TOP HALFSPACE FILE - contains the velocity, density, and incident angle within the material comprising the top halfspace of the multilayered structure. This file is a required input within the module ZLAYER.

BOTTOM HALFSPACE FILE - contains the velocity, density and wave of interest in the material comprising the bottom halfspace of the multilayered structure. This file is also a required input within the module ZLAYER.

MULTILAYER FILE - will ultimately contain the reflection and transmission coefficients for each layer as well as initial layer information (thickness, velocity, density, and wave of interest in layer). The program user has the option to either generate the coefficients for a new multilayered environment within the model, or to use a pre-created file. Data within this file is used to generate the waveform response.

WAVEFORM FILE - is the output file that contains the real, imaginary and absolute value parts of the waveform response for the given multilayered structure. The program user is prompted for the file name within ZLAYER.